Two-dimensional quantum central limit theorem by quantum walks

Keisuke Asahara [1,*] Daiju Funakawa [2,†] Motoki Seki [3,‡] and Akito Suzuki [4,§]

[1]*Education and Research Center for Mathematical and Data Science, Hokkaido University, Kita 12, Nishi 7, Kita-ku, Sapporo, Hokkaido 060-0812, Japan*

[2]*Department of Electronics and Information Engineering, Hokkai-Gakuen University, Sapporo, Hokkaido 062-8605, Japan*

[3]*Department of Mathematics, Faculty of Science, Hokkaido University, Sapporo 060-0810, Japan*

[4]*Department of Production Systems Engineering and Sciences, Komatsu University, Awazu Campus, Nu 1-3 Shicho-machi, Komatsu, Ishikawa 923-8511, Japan*

(Received 14 November 2025; accepted 2 February 2026; published 23 February 2026)

The weak limit theorem (WLT), the quantum analog of the central limit theorem, is foundational to quantum walk (QW) theory. Unlike the universal Gaussian limit of classical walks, deriving analytical forms of the limiting probability density function (PDF) in higher dimensions has remained a challenge since the one-dimensional (1D) Konno distribution was established. Previous explicit PDFs for two-dimensional (2D) models were limited to specific cases whose fundamental nature was unclear. This paper resolves this long-standing gap by introducing the notion of maximal speed $v_{\max}$ as a critical parameter. We demonstrate that all previous 2D solutions correspond to a degenerate regime where $v_{\max} = 1$. We then present the first exact analytical representation of the limiting PDF for the physically richer, unexplored regime $v_{\max} < 1$ of a general class of 2D two-state QWs. Our result reveals 2D Konno functions that govern these dynamics. We establish these as the proper 2D generalization of the 1D Konno distribution by demonstrating their convergence to the 1D form in the appropriate limit. Furthermore, our derivation, based on spectral analysis of the group-velocity map, analytically resolves the singular asymptotic structure: we explicitly determine the caustics loci where the PDF diverges and prove they define the boundaries of the distribution's support. By also providing a closed-form expression for the weight functions, this work offers a complete description of the 2D WLT.

DOI: 10.1103/fs8d-h2z8

I. INTRODUCTION

The central limit theorem (CLT) for classical random walks stands as a cornerstone of stochastic modeling, underpinning their vast applications [1–6]. Inspired by this classical success, and fueled by the rise of quantum computation [7–16], quantum walks (QWs) were introduced as their quantum counterpart [17–20]. QWs have proven to be a powerful resource, demonstrating capabilities for universal quantum computation [21–23] and offering new paradigms for quantum algorithms [24–27] and the simulation of physical phenomena [28–34].

Given the foundational role of the CLT, establishing its quantum analog—the weak limit theorem (WLT)—has been a central goal since Konno's pioneering one-dimensional (1D) analyses [35,36], which initiated an extensive line of inquiry [37–70]. However, the analogy is not straightforward. The WLT exhibits a rich, nontrivial structure, departing fundamentally from the universal Gaussian limit of the CLT. While this structure is now well-understood in 1D through the Konno distribution, its generalization to higher dimensions has proven far more challenging.

Despite this two-decade effort, progress in higher dimensions remained limited; while explicit probability density functions (PDFs) were derived for some specific two-dimensional (2D) models, their fundamental nature and relation to the 1D case were unclear [71,72].

A key contribution of this paper is to demonstrate, by introducing a notion of maximal speed $v_{\max}$, that all these previous 2D solutions correspond to a degenerate regime where $v_{\max} = 1$. Consequently, the physically richer, nontrivial regime $v_{\max} < 1$—which constitutes the proper 2D generalization of the 1D Konno distribution—had remained an entirely open problem since the original 1D work.

This paper directly addresses this long-standing gap. We present the first exact analytical representation of the limiting PDF for a general class of 2D two-state QWs (2D2SQWs), resolving their asymptotic behavior in the nontrivial regime $v_{\max} < 1$ and providing a complete description of the limit distribution.

A. Weak limit theorems

To fully appreciate the significance of this 2D generalization, we begin by reviewing the foundational 1D WLT. This

*Contact author: keisuke-asahara@mdsc.hokudai.ac.jp
†Contact author: funakawa@hgu.jp
‡Contact author: marmot.motoki@gmail.com
§Contact author: akito.suzuki@komatsu-u.ac.jp

Published by the American Physical Society under the terms of the Creative Commons Attribution 4.0 International license. Further distribution of this work must maintain attribution to the author(s) and the published article's title, journal citation, and DOI.

TABLE I. Distribution of V and corresponding asymptotic behaviors of 1D2SQW. Here, δ_a denotes the Dirac measure: $\delta_a(B) = 1$ if $a \in B$; 0 otherwise.

Maximal speed	Distribution of V	Asymptotic behavior
(a) $v_{\max} = 0$	δ_0	Bound in a region
(b) $v_{\max} = 1$	$C_{+1}\delta_{+1} + C_{-1}\delta_{-1}$	Trivial ballistic motion
(c) $v_{\max} \in (0, 1)$	$w(v) f_{\mathrm{K}}(v; v_{\max})$	Linear spreading

line of inquiry, which seeks a quantum analog of the CLT, was first pursued by Konno [35,36] as a WLT for a 1D two-state QW (1D2SQW), which states that the average displacement of the position X_t for a walker during t steps converges weakly to the asymptotic velocity V as $t \to \infty$.

The long-time asymptotic behavior of QWs can be rigorously separated into three types by introducing the maximal speed, $v_{\max} \in [0, 1]$, derived from the group velocity $v = d\omega/dk$ (defined by the dispersion relation ω) [73–75]. This parametrization allows for a clear summary of the 1D behaviors in Table I [36,76].

We first explain the cases of (a) and (b), which exhibit exceptional phenomena [63,65,66].

(a) *Bound in a finite region.* In the case of $v_{\max} = 0$, the asymptotic velocity is zero with probability one, i.e., $P(V = 0) = 1$. This phenomenon, sometimes referred to as localization [38,77], comes from the evolution operator having only eigenvalues, and thus the walker can only take a superposition of bound states, which means that the walker can hardly escape a sufficiently large finite region (see [78], Theorem 8.1] for instance).

(b) *Trivial ballistic motion.* The case of $v_{\max} = 1$ only allows the walker to move in a single direction. If the walker starts to move to the left (or right), the walker always moves to the left (or right). This phenomenon comes from the no-go lemma [29] which states in our setting that all scalar homogeneous unitary QWs are trivial; that is, the walker can move in a single direction. In fact, in the case of $v_{\max} = 1$, the evolution operator can be represented as the direct sum of two homogeneous unitary QWs without any inner degree of freedom.

(c) *Linear spreading.* Among these cases listed in Table I, the parameter regime $v_{\max} \in (0, 1)$ reveals the typical behavior of the QW. The asymptotic velocity V in this regime follows the Konno distribution:

$$P(V \leqslant u) = \lim_{t\to\infty} P\left(\frac{X_t}{t} \leqslant u\right) = \int_{-\infty}^{u} w(v) f_{\mathrm{K}}(v; v_{\max}) dv, \tag{1}$$

where the function f_{K} is the Konno function, defined as

$$f_{\mathrm{K}}(v; r) := \frac{\sqrt{1-r^2}}{\pi(1-v^2)\sqrt{r^2-v^2}} I_{(-r,r)}(v), \tag{2}$$

with $r \in (0, 1)$ being a parameter and I_S is the indicator function of a set S. Crucially, while the maximal speed $v_{\max}$ and the Konno function f_{K} are independent of the initial state, the function w carries all the information about the initial state in the distribution (1). Assuming that the walker starts at the origin with the initial qubit state $\alpha|0\rangle + \beta|1\rangle$, we can interpret the original result by Konno [35,36] in terms of effective mass $m_{\mathrm{eff}} = (d^2\omega/dk^2|_{k=0})^{-1}$ [75] as

$$w(v) = 1 - [|\alpha|^2 - |\beta|^2 + (\bar{\alpha}\beta + \bar{\beta}\alpha) m_{\mathrm{eff}}] v. \tag{3}$$

For the initial state of the form $\psi \otimes (\alpha|0\rangle + \beta|1\rangle)$, Machida [55] constructed interesting examples of explicit expressions for $w(v)$ by choosing functions ψ appropriately.

However, for a general initial state Ψ_0, determining $w(v)$ requires knowledge of the dynamics of the QW, since the probability density function (PDF) of the asymptotic velocity V is given by the spectral measure [79], formally written as $|\langle v|\Psi_0\rangle|^2 dv$, of the velocity operator $\hat{v}$ [37,63,65] associated with Ψ_0. The 1D2SQW consists of two wave packets corresponding to the two modes of frequencies $\pm\omega$, which inevitably makes the group velocity v a two-valued function $v_\pm(k)$ of the wave number $k \in \mathbb{T}$. Since each $v_\pm$ serves as a covering projection from $\mathbb{T}$ to the velocity domain $|v| \leqslant v_{\max}$, the wave-number space must be partitioned into injective regions $\mathbb{T} = \mathbb{T}_0 \cup \mathbb{T}_1$ to properly define the single-valued inverse functions $k = k_{\star,m}(v) := v_\star|^{-1}_{\mathbb{T}_m}(v)$ ($\star = \pm$, $m = 0, 1$). The rigorous application of the spectral analysis establishes the following closed expression for $w(v)$ (see Ref. [66] for details):

$$w(v) = \frac{1}{2} \sum_{\substack{\star=\pm \\ m=0,1}} P_\star(k_{\star,m}(v)), \tag{4}$$

where $P_\star(k)$ is a function calculated by the initial state. The derivatives of the inverse functions $k_{\star,m}$ derive the Konno function (2) up to a constant factor.

B. Finding 2D Konno function

As mentioned, the generalization of the 1D Konno distribution to higher dimensions has been a long-standing challenge. A critical distinction must be made here: while the WLT, which only ensures the existence of the limit, has been proven for broad classes of multidimensional QWs [37,80], the explicit analytical forms of their limiting PDFs have remained elusive.

To date, explicit analytical expressions for the limiting PDF have been derived only for the specific 2DQW models analyzed by Watabe *et al.* [71] and Di Franco *et al.* [72]. They derived the following 2D function $f(\boldsymbol{v})$ for these models:

$$f(\boldsymbol{v}) = \frac{1}{\pi^2(1-v_1^2)(1-v_2^2)} I_E(\boldsymbol{v}), \tag{5}$$

where E is an elliptic region given by

$$E = \left\{ \boldsymbol{v} = (v_1, v_2) \,\middle|\, \frac{(v_1+v_2)^2}{4a} + \frac{(v_1-v_2)^2}{4b} \leqslant 1 \right\}, \tag{6}$$

with a pair (a, b) of constants satisfying $a + b = 1$. As will be proved later, taking the 1D limit of Eq. (5) results in the trivial ballistic behavior of $v_{\max} = 1$, rather than the linear spreading described by the Konno function f_{K} for $v_{\max} \in (0, 1)$. Moreover, the accompanying challenge of analytically determining the initial-state-dependent function w for general initial states remains unaddressed.

This task is formidable, as the complexity of the spectral structure of the 2D velocity operator—which involves summing over multiple inverse velocity branches (four branches in the 1D case [66])—-grows with dimension. Unlike the 1D case where the velocity map $v_\pm(k)$ is a relatively simple covering, the 2D group velocity map $\boldsymbol{v}_\pm(\boldsymbol{k})$ is a highly noninjective 2D-to-2D transformation. Deriving w requires a complete spectral analysis, which hinges on inverting this map. This inversion is critically complicated by the presence of caustics—loci in the velocity space corresponding to points $\boldsymbol{k}$ where the Jacobian of the velocity map vanishes (i.e., the effective-mass tensor diverges [81]). These caustics manifest as divergences in the limiting PDF and, as suggested by Ahlbrecht *et al.* [81] via numerical analysis, define the boundaries of the PDF's support. However, an analytical resolution of this singular structure for a general 2DQW has remained elusive.

This critical omission, combined with the disconnection between f and f_{K}, raises fundamental questions:

(1) What is a proper 2D generalization of the Konno function f_{K}?

(2) What is a closed form of the weight function w?

(3) Can the singular asymptotic structure (the caustics and the PDF support) be determined analytically?

This work addresses these questions by first identifying the parameter constraint $a+b=1$ of the known 2DQW models [71,72] with the maximal speed, $v_{\max}=a+b$. This identification reveals that previous analytical studies were confined to the $v_{\max}=1$ regime. As we prove, this regime, when taken to the proper 1D limit, degenerates into the trivial ballistic motion of a 1D QW, in sharp contrast to the linear spreading regime described by the Konno distribution [see Table I, rows (b) and (c)].

We therefore address these fundamental questions by providing the first analytical solution for the unexplored, nontrivial regime $v_{\max}=a+b<1$. Our main contributions are threefold, corresponding directly to the questions above:

(1) We obtain the exact representation of the 2D Konno functions $f_\pm$ for unexplored regime $v_{\max}<1$, addressing question 1. We rigorously establish these as the proper 2D generalization of the Konno function by demonstrating their convergence back to the 1D Konno function f_{K} in the appropriate 1D limit, whereas the known PDF (2) degenerates to the trivial ballistic model.

(2) We provide a complete description of the limit distribution by deriving the closed-form expression for the weight function $w(v)$ for both regimes $v_{\max}\leqslant 1$, thereby resolving question 2.

(3) Our thorough spectral analysis provides the first complete analytical resolution of the 2DQW's singular asymptotic structure, addressing question 3. We explicitly determine the caustics loci where the Jacobian vanishes, and the PDF diverges, and prove they define the boundaries of the PDF's support. This analytically generalizes what was previously suggested numerically [81].

The remainder of this paper is organized as follows: In Sec. II, we introduce our 2DQW model and characterize it with a pair of parameters (a,b), which define the maximal speed $v_{\max}=a+b$. Section III presents our main results, deriving the limiting PDFs for both parameter regimes: For $v_{\max}\in(0,1)$, we derive the 2D Konno functions $f_\pm$ (Theorem 1). For $v_{\max}=1$, we recover the known function f (Theorem 3). Here, we also provide the rigorous 1D limit theorems for the entire distribution. We prove that the $v_{\max}<1$ regime properly converges to the 1D Konno distribution (Theorem 2), while the $v_{\max}=1$ regime degenerates to trivial ballistic motion (Theorem 4). These theorems establish contribution (1). Section IV validates and discusses the implications of these results. We compare our findings with previous studies. We then analyze the convergence mechanism of the 2D functions $f_\pm$ themselves in Sec. IV A, detailing how their support deforms (Fig. 5) to recover the 1D Konno function f_{K}. Section IV B discusses the physical implications of our analytical resolution of the singular asymptotics. Section V sketches the proofs for the main theorems. This section details the technical achievement of our work: the spectral analysis of the velocity map, the handling of the Jacobian, and the identification of caustics (Theorem 7), which completes contribution (3); and the final derivation of the closed-form weight function $w(v)$ [(46) in Sec. V E], which achieves contribution (2). Section VI concludes this paper. The appendixes contain detailed proofs of propositions and additional supporting results.

II. MODELS

This paper investigates a homogeneous 2D two-state QW (2D2SQW), a model initially defined by Di Franco *et al.* [82], and referred to as the alternate QW (AQW) [82]. This model was originally introduced to realize 2D four-state QWs (2D4SQWs) [77] such as the Grover walk [83] with fewer experimental resources. We treat a slightly generalized version of the 2D2SQW model. As will be shown, this modification provides rich phenomena for the asymptotic behavior of the walker, enabling the explicit derivation of the 2D Konno function.

A. Probability and dynamics

We consider a walker moving on the 2D square lattice $\mathbb{Z}^2=\{\boldsymbol{x}=(x_1,x_2)\mid x_1,x_2\in\mathbb{Z}\}$. The position $\boldsymbol{X}_t$ of the walker at time $t=0,1,2,\ldots$ follows the probability distribution:

$$P(\boldsymbol{X}_t=\boldsymbol{x})=\Psi_t^\dagger(\boldsymbol{x})\Psi_t(\boldsymbol{x}),\quad \boldsymbol{x}\in\mathbb{Z}^2, \tag{7}$$

where the $\mathbb{C}^2$-valued function

$$\Psi_t(\boldsymbol{x})=\begin{pmatrix}\Psi_t^{(+)}(\boldsymbol{x})\\ \Psi_t^{(-)}(\boldsymbol{x})\end{pmatrix}$$

represents the state of the walker with each component $\Psi_t^{(\pm)}(\boldsymbol{x})$ denoting the walker's inner degrees of freedom. The Hilbert space of states of the walker is thus the set of $\mathcal{H}:=\ell^2(\mathbb{Z}^2;\mathbb{C}^2)\simeq\ell^2(\mathbb{Z}^2)\otimes\mathbb{C}^2$, where $\ell^2(\mathbb{Z}^2)$ is the Hilbert space of square summable functions from $\mathbb{Z}^2$ to $\mathbb{C}$. The state evolution of the 2D2SQW is then defined by the recurrence relation:

$$\Psi_{t+1}(\boldsymbol{x})=\sum_{s\in\{(s_1,s_2)\mid s_j=-1,+1\}}Q_s\Psi_t(\boldsymbol{x}-\boldsymbol{s}) \tag{8}$$

for $\boldsymbol{x}\in\mathbb{Z}^2$ and $t=0,1,2,\ldots$. This provides a quantum analog of the difference equation that governs the probability distribution of a 2D random walk. In (8), the two-by-two matrices Q_s are assumed to be independent of the position, which

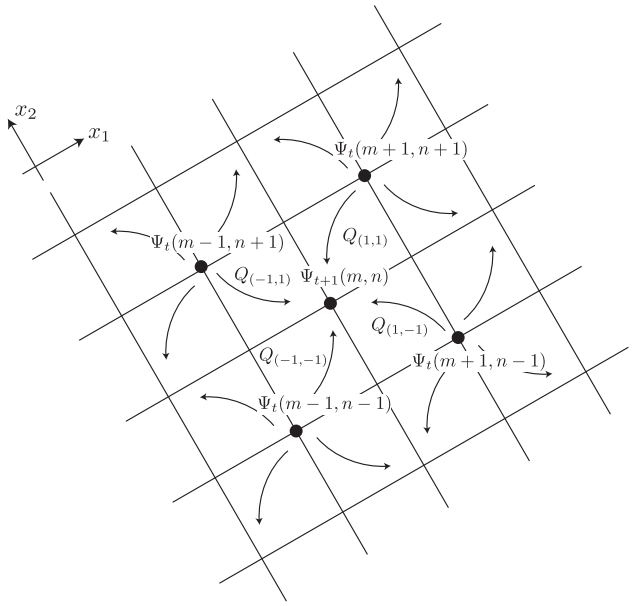


FIG. 1. The walker in $\mathbb{Z}^2$ that follows (8).

implies that the evolution described by (8) is homogeneous or, equivalently, translation invariant. See Fig. 1 for the motion of the 2D2SQW in $\mathbb{Z}^2$.

Ohno [84] provided a criterion for the translation-invariant 2D2SQW of the form (8) to be unitary. Based on this criterion, one can rewrite all such unitary evolutions as

$$\Psi_{t+1} = U\Psi_t, \quad t = 0, 1, 2, \ldots, \tag{9}$$

where Ψ_0 is the initial state and the unitary evolution operator U is given by the product of conditional shift operators S_j and coin operators C_j $(j = 1, 2)$:

$$U := S_2 C_2 S_1 C_1. \tag{10}$$

The action of S_j $(j = 1, 2)$ is defined on a state $\Psi \in \mathcal{H}$ by $(S_j\Psi)^{(\pm)}(\boldsymbol{x}) = \Psi^{(\pm)}(\boldsymbol{x} \pm \boldsymbol{e}_j)$ with the standard basis $\{\boldsymbol{e}_j\}_{j=1,2}$. The coin operators C_j are taken as arbitrary two-by-two unitary matrices, and they are naturally identified with the operator $I \otimes C_j$ $(j = 1, 2)$ on the full Hilbert space $\mathcal{H}$ by omitting the identity I. The relation $\sum_{\boldsymbol{s}\in\{(s_1,s_2)|s_j=-1,+1\}} Q_{\boldsymbol{s}} = C_2C_1$ between the transition matrices $Q_{\boldsymbol{s}}$ and the coin matrices C_j, along with the unitarity of C_j, guarantees the unitarity of the evolution U and thus the state evolution (8). This is the quantum analogy of probability conservation in the classical random walk; that is, the sum of the probability of moving from $\boldsymbol{x} - \boldsymbol{s}$ to $\boldsymbol{x}$ over all allowed displacements $\boldsymbol{s} \in \{(s_1, s_2) \mid s_j = -1, +1\}$ equals one.

B. Parameters

In general, any two-by-two unitary matrices $C \in U(2)$ are parametrized by one real number $r \in [0, 1]$ and three angles $\alpha, \beta, \delta \in [-\pi, \pi)$ as

$$C = C(r; \alpha, \beta, \delta) := e^{i\delta/2}\begin{pmatrix} e^{i\alpha}r & e^{i\beta}s \\ -e^{-i\beta}s & e^{-i\alpha}r \end{pmatrix},$$

with $s = (1 - r^2)^{1/2}$ and $\det C = e^{i\delta}$. The following lemma then reduces the parameters and leads to a canonical form of the coin operator C_j. The detailed proof is given in Appendix A 1.

Lemma 1. Fix $a_j \in [0, 1]$ and $\alpha_j, \beta_j, \delta_j \in [-\pi, \pi)$ $(j = 1, 2)$. Let U be the operator defined by (10) with coin operators given by

$$C_j = C(a_j; 0, 0, 0) \quad (j = 1, 2),$$

and $U' := S_2C_2'S_1C_1'$ with

$$C_j' = C(a_j; \alpha_j, \beta_j, \delta_j) \quad (j = 1, 2).$$

Then there exists a unitary operator W on $\mathcal{H}$ such that the following hold:

(i) There exists a constant $\gamma \in [-\pi, \pi)$ such that

$$W^\dagger U' W = e^{i\gamma} U,$$

i.e., U' and U are unitarily equivalent up to a constant factor.

(ii) Let $\Psi_t' = (U')^t\Psi_0'$ with $\|\Psi_0'\| = 1$ and define the position $\boldsymbol{X}_t'$ in the same manner as (7) with Ψ_t replaced by Ψ_t'. Then $\boldsymbol{X}_t'$ has the same distribution as $\boldsymbol{X}_t$ defined by (7) with $\Psi_0 = W^\dagger\Psi_0'$, i.e.,

$$P(\boldsymbol{X}_t' = \boldsymbol{x}) = P(\boldsymbol{X}_t = \boldsymbol{x}), \quad \boldsymbol{x} \in \mathbb{Z}^2$$

for any $t = 0, 1, 2, \ldots$.

From Lemma 1, the probability distribution (7) of the position $\boldsymbol{X}_t$ is independent of the phase angles $\alpha_j, \beta_j, \delta_j \in [-\pi, \pi)$ $(j = 1, 2)$. Consequently, the limit distribution is also independent of these angles. Without loss of generality, we can, therefore, suppose that the coin operators are of the simpler canonical form:

$$C_j = C(a_j; 0, 0, 0) = \begin{pmatrix} a_j & b_j \\ -b_j & a_j \end{pmatrix}, \tag{11}$$

with $a_j \in [0, 1]$ and $b_j = (1 - a_j^2)^{1/2}$. Thus, the translation-invariant 2D2SQW model treated in this paper is fully parametrized by only two real numbers $a_1, a_2 \in [0, 1]$, which coincides with Ohno's result [84].

To facilitate the presentation of the main results, we parametrize our model using two quantities, a and b, derived from (11) by

$$a := a_2a_1, \quad b := b_2b_1. \tag{12}$$

By definition, the resulting pair (a, b) of parameters must be in the triangular region Δ defined by the three constraints (depicted in Fig. 2):

$$\Delta = \{(a, b) \mid a \geqslant 0,\ b \geqslant 0,\ a + b \leqslant 1\}.$$

The following lemma ensures that Δ provides a nonredundant parametrization of our model by establishing a one-to-one correspondence between the ordered coin parameters (a_1, a_2) and $(a, b) \in \Delta$. The proof is deferred to Appendix A 2.

Lemma 2. For $(i, j) = (1, 2)$ or $(2, 1)$, let $A_{ij} = \{(a_1, a_2) \mid 0 \leqslant a_i \leqslant a_j \leqslant 1\}$. Define maps

$$\Phi_{ij} : A_{ij} \ni (a_1, a_2) \longmapsto (a, b) \in \Delta$$

so that (a, b) satisfies (12). Then Φ_{ij} are one-to-one correspondences.

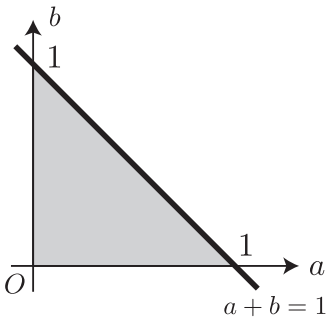


FIG. 2. Parameter region for $(a, b) \in \Delta$. The parameter pair can take any value within the interior of the gray-shaded triangle and its boundary, where $a + b = 1$.

III. RESULTS

This paper derives an explicit expression for the limiting PDF of the scaled position $\boldsymbol{X}_t/t$ for translation-invariant 2D2SQWs parametrized by (a, b) in the region depicted in Fig. 2. By Lemma 1, one can assume, without loss of generality, that the evolution operator $U = S_2C_2S_1C_1$ has coin operators C_j of the canonical form (11). The state Ψ_t of the walker at time $t = 0, 1, 2, \ldots$ is given by (9): $\Psi_t = U^t\Psi_0$, where the initial state $\Psi_0 \in \mathcal{H}$ is an arbitrary normalized vector. The probability distribution $P(\boldsymbol{X}_t = \boldsymbol{x})$ is obtained from the state $\Psi_t(\boldsymbol{x})$ via (7). Lemma 2 ensures that $(a, b) \in \Delta$ fully determines the model through $a = a_1a_2$ and $b = b_1b_2$.

According to Ref. [37], the limit distribution is given by

$$P(V_1 \leqslant u_1, V_2 \leqslant u_2) = \int_{-\infty}^{u_1}\int_{-\infty}^{u_2} d\langle\Psi_0|E_{\hat{\boldsymbol{v}}}(\boldsymbol{v})\Psi_0\rangle,$$

where $E_{\hat{\boldsymbol{v}}} = E_{\hat{v}_1} \otimes E_{\hat{v}_2}$ denotes the (joint) spectral measure for the (pair of asymptotic) velocity operators $\hat{\boldsymbol{v}} = (\hat{v}_1, \hat{v}_2)$. and one may formally represent $\langle\Psi_0|E_{\hat{\boldsymbol{v}}}(\boldsymbol{v})\Psi_0\rangle$ as $|\langle\boldsymbol{v}|\Psi_0\rangle|^2$ (see Sec. V for the precise definition). Intuitively, in the wave-vector space representation, the velocity operators $\boldsymbol{v}(\boldsymbol{k}) = (v_1(\boldsymbol{k}), v_2(\boldsymbol{k}))$ are equal to the group velocity, $\boldsymbol{v}(\boldsymbol{k}) = \nabla\omega$, whose ranges determine the spectra $\sigma(\hat{\boldsymbol{v}}_j)$. Here, $\omega(\boldsymbol{k})$ denotes the dispersion relation of our model, which satisfies $\cos\omega(\boldsymbol{k}) = \tau(\boldsymbol{k})$ with

$$\tau(\boldsymbol{k}) = a\cos(k_2 + k_1) - b\cos(k_2 - k_1) \tag{13}$$

for the wave vector $\boldsymbol{k} = (k_1, k_2) \in \mathbb{T}^2$.

A. Maximal speeds and parameters

As in the 1DQW model, the maximal speed plays a key role in characterizing the limit distribution and the asymptotic behavior. We thus define the maximal speed of the 2D2SQW as

$$v_{\max} := \max_{j=1,2}\max_{\boldsymbol{k}\in\mathbb{T}^2}|v_j(\boldsymbol{k})|.$$

Expressing v_j in terms of the function $\tau(\boldsymbol{k})$ and its derivatives, we can determine the spectra $\sigma(\hat{v}_j)$ and the maximal speed $v_{\max}$. The explicit result is given by the following proposition:

Proposition 1 (Maximal speed). The following hold:

(i) $v_{\max} = a + b$.

(ii) $\sigma(\hat{v}_j) = [-v_{\max}, v_{\max}]$ for $j = 1, 2$.

TABLE II. Complete list of choices of (a_1, a_2) corresponding to $(a, b) \in \Delta_{ab=0}$. The action of $\tilde{S}_{1D} = S_2S_1$ on $\ell_2(\mathbb{L}_n^{(+)}; \mathbb{C}^2)$ parallels the action of S_{1D} on $\ell_2(\mathbb{L}_n^{(-)}; \mathbb{C}^2)$.

Choice	$v_{\max}$	1D decomposition	Lines
$a_1 = 1$	$a = a_2$	$\tilde{S}_{1D}C_2$	$\mathbb{L}_n^{(+)}$
$a_2 = 1$	$a = a_1$	$\tilde{S}_{1D}C_1$	$\mathbb{L}_n^{(+)}$
$a_1 = 0$	$b = b_2$	$S_{1D}\tilde{C}_2$	$\mathbb{L}_n^{(-)}$
$a_2 = 0$	$b = b_1$	$S_{1D}^\dagger\tilde{C}_1$	$\mathbb{L}_n^{(-)}$

As shown later, the support of the limit distribution equals the support $\Sigma(\hat{\boldsymbol{v}})$ of the joint spectral measure $E_{\hat{\boldsymbol{v}}}$. In general, the joint spectrum $\Sigma(\hat{\boldsymbol{v}})$ is strictly contained in the Cartesian product of the spectra $\sigma(\hat{v}_j)$ (see Sec. V A for more details): $\Sigma(\hat{\boldsymbol{v}}) \subset \sigma(\hat{v}_1) \times \sigma(\hat{v}_2)$.

Di Franco *et al.* [72] showed that, for AQWs with $v_{\max} = 1$, $\Sigma(\hat{\boldsymbol{v}})$ consists of a single ellipse E given in (6). More recently, Cedzich *et al.* [85], Sec. 5.2] reported a model, corresponding to the $a = b = 1/2$ case of our general framework, where $\Sigma(\hat{\boldsymbol{v}})$ becomes a unit circle and $v_{\max} = 1$. As suggested in [81], Fig. 4(b)], for an AQW with $v_{\max} < 1$, $\Sigma(\hat{\boldsymbol{v}})$ appears to be the intersection of two elliptical regions. These facts suggest the necessity of dividing the parameter region of (a, b) into several distinct cases. We thus define three regions $\Delta_{ab=0}$, $\Delta_{(0,1)}$, and Δ_1 of the parameters Δ as

$$\Delta_{ab=0} = \{(a, b) \in \Delta \mid ab = 0\},$$
$$\Delta_{(0,1)} = \{(a, b) \in \Delta \mid\ a + b < 1,\ ab \neq 0\},$$
$$\Delta_1 = \{(a, b) \in \Delta \mid a + b = 1,\ ab \neq 0\}.$$

B. Regime of reducible QWs: $\Delta_{ab=0}$

If the parameters satisfy $(a, b) \in \Delta_{ab=0}$, our model can be reduced to two simpler scenarios:

(i) The walker exhibits $v_{\max} = 0$ if and only if $a = b = 0$. In this case, the walker is bound in a finite region, which corresponds to row (a) of Table I for the 1D2SQW.

(ii) The walker has nonzero velocity, i.e., $v_{\max} \in (0, 1)$, but the parameters are supposed to satisfy either $a = 0$ or $b = 0$. For instance, in the case where $a_1 = 0$, i.e., $a = 0$ and $b = b_2$, one can prove, by a method similar to Lemma 1, that U is unitarily equivalent to the decoupled form:

$$U \simeq \bigoplus_{n\in\mathbb{Z}} S_{1D}\tilde{C}_2 \text{ on } \bigoplus_{n\in\mathbb{Z}} \ell^2(\mathbb{L}_n^{(-)}; \mathbb{C}^2),$$

where the walker's motion is constrained to each line $\mathbb{L}_n^{(-)}$ $(n \in \mathbb{Z})$. Here we use $\mathbb{L}_n^{(\pm)}$ to denote the line:

$$\mathbb{L}_n^{(\pm)} = \{(m, n \pm m) \mid m \in \mathbb{Z}\} \subset \mathbb{Z}^2 \quad (n \in \mathbb{Z}),$$

and identify $\mathbb{L}_n^{(\pm)}$ with $\mathbb{Z}$ in a natural way such that $(m, n \pm m) \mapsto m$. In the above decomposition, the action of the operator $S_{1D} = S_2^\dagger S_1$ on $\ell^2(\mathbb{L}_n^{(-)}; \mathbb{C}^2)$ is represented as $(S_{1D}\Psi)^{(\pm)}(m) = \Psi^{(\pm)}(m \pm 1)$. Also, the symbol $\tilde{C}_j$ denotes $C(b_j; \pi, 0, 0)$.

Table II summarizes the complete set of decompositions for all choices in $\Delta_{ab=0}$, confirming that the resulting 1D distributions on each line are given established 1D WLT results in Table I.

In subsequent sections, we therefore focus our analysis exclusively on the case where $ab \neq 0$, which corresponds to the intrinsically 2D motion of the walker.

C. Regime of Konno functions: $\Delta_{(0,1)}$

This section supposes that

$$(a, b) \in \Delta_{(0,1)}, \text{ i.e., } v_{\max} \in (0, 1), \quad ab \neq 0.$$

Let F_j $(j = 1, 2)$ and F_0 be functions given by

$$F_j(\boldsymbol{v}) = 1 - \frac{(v_1 + v_2)^2}{4a_j^2} - \frac{(v_1 - v_2)^2}{4b_j^2},$$

$$F_0(\boldsymbol{v}) = \frac{(a_1b_2)^2 + (a_2b_1)^2}{2ab} \times \left[1 - \frac{(v_1 + v_2)^2}{4a_0^2} - \frac{(v_1 - v_2)^2}{4b_0^2}\right], \tag{14}$$

with

$$a_0^2 = \frac{(a_1b_2)^2 + (a_2b_1)^2}{b_1^2 + b_2^2}, \quad b_0^2 = \frac{(a_1b_2)^2 + (a_2b_1)^2}{a_1^2 + a_2^2},$$

and denote by E_j the ellipses defined by F_j:

$$E_j = \{\boldsymbol{v} = (v_1, v_2) \,|\, F_j(\boldsymbol{v}) \geqslant 0\}. \tag{15}$$

We now present our main result:

Theorem 1 (2D Konno functions). Suppose that $(a, b) \in \Delta_{(0,1)}$. Then the limiting distribution of $\boldsymbol{X}_t/t$ is given by

$$P(V_1 \leqslant u_1, V_2 \leqslant u_2) = \int_{-\infty}^{u_1}\int_{-\infty}^{u_2} dv_1 dv_2 \sum_{\bullet=\pm} w_\bullet(\boldsymbol{v}) f_\bullet(\boldsymbol{v}),$$

where $w_\pm$ are weight functions defined in (46), and $f_\pm$ are state-independent functions defined as

$$f_\pm = \frac{F_0 \pm \sqrt{F_1F_2}}{2\pi^2(1 - v_1^2)(1 - v_2^2)\sqrt{F_1F_2}} I_{E_1 \cap E_2}. \tag{16}$$

We sketch the proof of Theorem 1 in Sec. V. From Lemma 3 (proved in Appendix A 3) below, $f_\pm$ are well defined, strictly positive in the interior of $E_1 \cap E_2$, and $f_\pm$ diverge only on the boundary of $E_1 \cap E_2$.

Lemma 3. Let $(a, b) \in \Delta_{(0,1)}$.

(1) $F_1F_2 \geqslant 0$ in $E_1 \cap E_2$ and $F_1F_2 = 0$ only on the boundary of $E_1 \cap E_2$.

(2) $F_0 > \sqrt{F_1F_2}$ in $E_1 \cap E_2$.

(3) $(1 - v_1^2)(1 - v_2^2) > 0$ in $E_1 \cap E_2$.

Figure 3 depicts the domain of $f_\pm$. In particular, the domain of the PDF is $E_1 \cap E_2$, independent of the initial state. Figure 4 shows the three-dimensional (3D) plot and the heat map of $f_\pm$. Especially, the fact that $f_\pm$ diverges on the boundary of $E_1 \cap E_2$ is consistent with Lemma 3.

1D limit to Konno function

To establish the connection between our 2D functions $f_\pm$ and the celebrated 1D Konno function (2), we define the appropriate reduction of our 2D model in the 1D limit. To make the dependence on $(a, b) \in \Delta$ clear, we use $U_{(a,b)}$ to denote the evolution operator $U = S_2C_2S_1C_1$ and we also denote the limiting PDF obtained in Theorem 1 by $\rho_{(a,b)}(\boldsymbol{v}) = \sum_{\bullet=\pm} w_\bullet(\boldsymbol{v}) f_\bullet(\boldsymbol{v})$. We use the notation from Lemma 2.

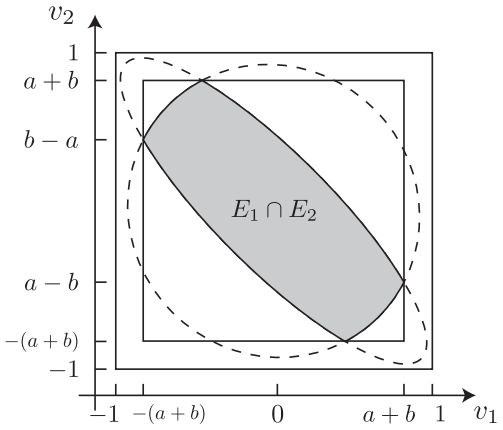


FIG. 3. The support of 2D Konno functions $f_\pm$ in (16) is $E_1 \cap E_2$, which is the intersection of two ellipses (whose boundaries are shown as dashed lines) and is colored gray. The region is plotted for $(a_1, a_2) = (1/4, 3/4)$, i.e., $(a, b) = (3/16, \sqrt{105}/16)$. In general, the domain $\Sigma(\hat{\boldsymbol{v}}) = E_1 \cap E_2$ is included in $\sigma(\hat{v}_1) \times \sigma(\hat{v}_2) = [-(a + b), a + b]^2$, which is also confirmed in this figure. In particular, $E_1 \cap E_2$ is contained in $[-1, 1]^2$, as visually confirmed in this figure, and therefore Lemma 3(3) holds.

Definition 1 (1D limit). Take $(a_1, a_2) = \Phi_{12}^{-1}((a, b))$ so that $(a, b) \in \Delta_{(0,1)}$ and fix a_1. We say that $\rho_{(a,b)}$ has the 1D limit if there exists a 1D PDF $\rho_{a_1}(v)$ such that

$$\lim_{b_2 \to 0} \int_{\Sigma(\hat{\boldsymbol{v}})} g(\boldsymbol{v}) \rho_{(a,b)}(\boldsymbol{v}) d\boldsymbol{v} = \int_{-a_1}^{a_1} g(v, v) \rho_{a_1}(v) dv \tag{17}$$

for any bounded continuous function $g(\boldsymbol{v})$. In this case, we write the limit as $\lim_{b \to 0} \rho_{(a,b)} = \rho_{a_1}$ and call it the 1D limit of $\rho_{(a,b)}$ as $b \to 0$.

The 1D limit procedure involves the following:

(1) The parameters (a, b) remain strictly within the regime $\Delta_{(0,1)}$ as they approach the boundary $\Delta_{ab=0}$, corresponding to $b_2 \to 0$ from above.

(2) Due to the limit $\lim_{b \to 0}(a, b) = (a_1, 0)$, the maximal speed $v_{\max} = a + b$ has a nonzero limit $a_1 \in (0, 1)$.

(3) The evolution $U_{(a,b)}$ converges to $U_{a_1} := S_2S_1C_1$, which represents a 1D motion along each line $\mathbb{L}_n^{(+)}$ $(n \in \mathbb{Z})$ (see Table II).

(4) The right-hand side (RHS) of (17) can formally be written as

$$\int_{\Sigma(\hat{\boldsymbol{v}})} g(\boldsymbol{v}) \delta(v_2 - v_1) \rho_{a_1}(v_1) \, d\boldsymbol{v}, \tag{18}$$

which implies that the 2D PDF $\rho_{(a,b)}$ degenerates in the 1D limit $b \to 0$.

The following theorem (proved in Appendix E) implies that our function $f_\pm$ converges to the 1D Konno function f_{K} in the 1D limit.

Theorem 2 (1D limit). Let $(a, b) \in \Delta_{(0,1)}$. Then $\rho_{a_1} := \lim_{b \to 0} \rho_{(a,b)}$ exists and

$$\rho_{a_1}(v) = w(v; a_1) f_{\mathrm{K}}(v; a_1), \tag{19}$$

where the weight function $w(\cdot; a_1)$ is defined in (E8).

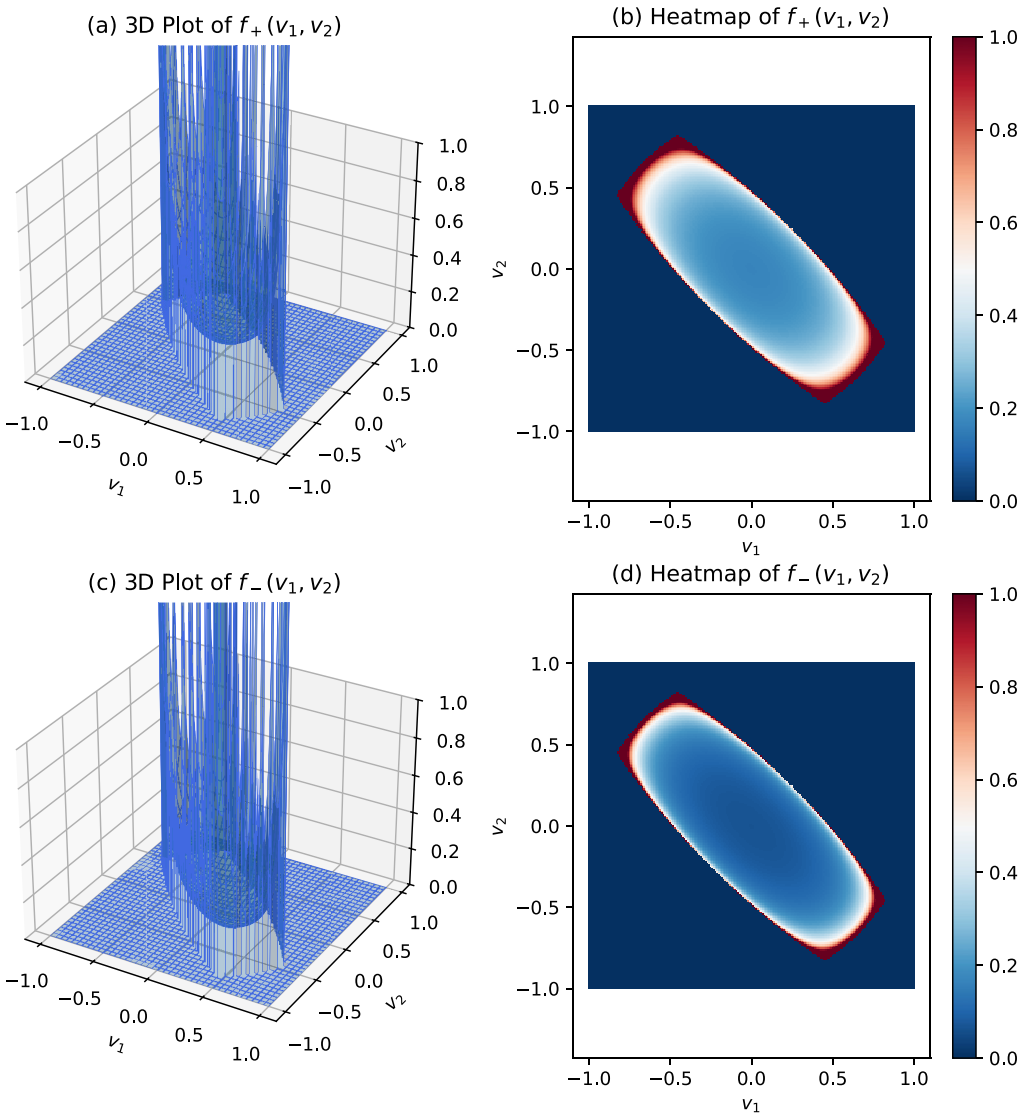


FIG. 4. Panels (a) and (c) show 3D plots of 2D Konno functions $f_+(\boldsymbol{v})$ and $f_-(\boldsymbol{v})$, respectively, for $(a_1, a_2) = (1/4, 3/4)$, i.e., $(a, b) = (3/16, \sqrt{105}/16)$, similar to Fig. 3. Panels (b) and (d) show the corresponding heat maps. In the heat maps, the color scale represents the function's value, which is zero (dark blue) outside the domain and increases toward the boundary (light blue through white to red), as indicated by the color bars. The set in panels (b) and (d) is identical to that in Fig. 3, and it can be seen that $f_\pm(\boldsymbol{v})$ diverges on this boundary. This fact corresponds to the divergence of 1D Konno function f_K at the points $v = \pm v_{\max}$.

This result confirms that our derived functions actually constitute the 2D generalization of the 1D Konno distribution, and therefore we refer to $f_\pm$ as the 2D Konno functions. We discuss how the 2D functions $f_\pm$ reduce to the Konno function f_K at the end of Sec. IV A.

D. Regime of maximal speed $v_{\max} = 1$: Δ_1

This section assumes that

$$(a, b) \in \Delta_1, \text{ i.e., } v_{\max} = 1, \quad ab \neq 0.$$

Equations (A1) and (A2) in Appendix A 2 prove that $a + b = 1$ if and only if $a_1 = a_2$ and $b_1 = b_2$. Recall that $F_j = 0$ defines the boundary of the ellipse E_j $(j = 1, 2)$ by (15). Similarly, F_0 defined in (14) also defines a boundary of an ellipse. The function

$$F(\boldsymbol{v}) = 1 - \frac{(v_1 + v_2)^2}{4a} - \frac{(v_1 - v_2)^2}{4b}$$

gives the boundary of the ellipse E defined in (6).

Lemma 4. Let $(a, b) \in \Delta_1$. Then,

(1) $F = F_j$ and hence $E = E_j$ $(j = 1, 2)$.

(2) $F = F_0$.

Proof. (1) is obvious from the relations $a = a_1^2 = a_2^2$ and $b = b_1^2 = b_2^2$. These relations also provide $a = a_0^2$, $b = b_0^2$, and $2ab = (a_1 b_2)^2 + (a_2 b_1)^2$. Substituting these relations into (14) yields (2). ■

Combining Lemma 4 with (16), we observe that f_+ coincides with f defined in (5), while f_- vanishes:

$$f_+ = f, \quad f_- = 0.$$

Lemma 4 also implies that the intersection of two ellipses $E_1 \cap E_2$, which constitutes the support of the 2D Konno function f_+, degenerates into the single ellipse E defined in (6): $E_1 \cap E_2 = E$.

Recall that f is the function defined in (5).

Theorem 3. Let $(a, b) \in \Delta_1$. Then the limit distribution of $\boldsymbol{X}_t/t$ is given by

$$P(V_1 \leqslant u_1, V_2 \leqslant u_2) = \int_{-\infty}^{u_1}\int_{-\infty}^{u_2} dv_1 dv_2\, w_+(\boldsymbol{v}) f(\boldsymbol{v}),$$

where the weight function w_+ is defined in Eq. (46).

Thus, we have recovered the function f obtained by Watabe *et al.* [71] and Di Franco *et al.* [72] as a special case of f_+ with $v_{\max} = 1$ and $ab \neq 0$. Although the statement of Theorem 3 might appear to be a straightforward corollary of Theorem 1 in light of Lemma 4, the proof requires a careful approach due to the discontinuity of the group velocity $\boldsymbol{v}(\boldsymbol{k})$. This kind of difficulty was previously noted in Ref. [37], Technical remark at the end of Sec. III]. We address this problem at the end of Sec. V E.

Triviality of the 1D limit

While the function $f_+ = f$ in the Δ_1 regime recovers the prior studies [71,72], the following theorem reveals that f cannot be properly interpreted as a genuine 2D generalization of the Konno function; the 1D limit of the PDF in the Δ_1 regime becomes trivial.

Note that for $(a, b) \in \Delta_1$, the relation $b_2 = b_1 = \sqrt{b}$ holds, unlike the case for $(a, b) \in \Delta_{(0,1)}$. Hence, (a, b) converges to $(1, 0)$ as $b \to 0$ (or equivalently, $b_1 = b_2 \to 0$ and $a_1 = a_2 \to 1$). With this procedure, the evolution $U_{(a,b)} = S_2C_2S_1C_1$ converges to $U_1 = S_2S_1$, which is the 1D2SQW moving only in a single direction.

From these observations, Definition 1 requires the following modification for $(a, b) \in \Delta_1$: Let $\rho^{(1)}_{(a,b)} = w_+ f$ be the PDF obtained by Theorem 3. We say that $\rho^{(1)}_{(a,b)}$ has the 1D limit if there exists a 1D distribution (generalized function) $\rho_1(v)$, understood as a measure, such that

$$\lim_{b_2 \to 0} \int_{\Sigma(\hat{\boldsymbol{v}})} g(\boldsymbol{v}) \rho^{(1)}_{(a,b)}(\boldsymbol{v}) d\boldsymbol{v} = \int_{-1}^{1} g(v, v) \rho_1(v) dv$$

for any bounded continuous function $g(\boldsymbol{v})$. Similarly to (18), the integral on the RHS is formally interpreted as the action of the distribution $\delta(v_2 - v_1)\rho_1(v_1)$ on a test function g.

Theorem 4. Let $(a, b) \in \Delta_1$. Then $\rho_1 := \lim_{b \to 0} \rho^{(1)}_{(a,b)}$ exists and

$$\rho_1(v) = C_{-1}\delta_{-1}(v) + C_{+1}\delta_{+1}(v), \tag{20}$$

where the constants $C_{\pm 1} = \|\Psi_0^{(\mp)}\|^2_{\ell^2(\mathbb{Z}^2)}$.

Theorem 4 (proved in Appendix E) means that the 2D PDF $w_+ f$ degenerates to the 1D distribution corresponding to the trivial ballistic motion with $v_{\max} = 1$ [see Table I, row (b)]. We thus find that the function f (recovered from prior studies [71,72]) is a 2D generalization of the trivial 1D ballistic motion ($v_{\max} = 1$). This contrasts sharply with our 2D Konno functions $f_\pm$, which we have shown to be the genuine generalization of the nontrivial 1D Konno distribution ($v_{\max} < 1$).

TABLE III. Limit distributions and 1D limits.

(a, b)	$v_{\max}$	Distribution	1D limit
$\Delta_{ab=0}$	$\max\{a, b\}$	1D2SQW	
$\Delta_{(0,1)}$	$0 < a + b < 1$	$w_+f_+ + w_-f_-$	wf_{K}
Δ_1	1	w_+f	$C_{+1}\delta_{+1} + C_{-1}\delta_{-1}$

IV. DISCUSSION

This paper has dealt with 2D2SQW in a general form, successfully deriving the explicit limit PDF of $\boldsymbol{X}_t/t$, and clarifying its structural relation to the 1D2SQW. Table III summarizes the resulting distribution and its 1D limits for each parameter region in Δ.

A. How 2D functions reduce to Konno function

We have demonstrated in the previous section that the function f converges to trivial 1D dynamics in the 1D limit, while our 2D function $f_\pm$ converges to the Konno function f_{K}. The key distinction between $f_\pm$ and f arises from the presence of the factor:

$$K_\pm(\boldsymbol{v}; v_{\max}) = \frac{F_0 \pm \sqrt{F_1F_2}}{2\sqrt{F_1F_2}} I_{E_1 \cap E_2}.$$

When $v_{\max} = 1$, these factors formally become

$$K_+(\boldsymbol{v}; 1) = I_E(\boldsymbol{v}), \quad K_-(\boldsymbol{v}; 1) = 0,$$

leading to $E_1 \cap E_2 = E$, $f_+ \equiv f$, and $f_- \equiv 0$ (see Lemma 4 and the surrounding discussion).

The factor $K_\pm$ also provides a key to understanding the mechanism behind the convergence of the 2D Konno function $f_\pm$ to the 1D Konno function f_{K} in the 1D limit $b \to 0$. To analyze this limit, we introduce a change of variables that rotates the coordinate system by $\pi/4$: $v = (v_1 + v_2)/2$, $u = (v_1 - v_2)/2$. We define

$$\tilde{K}_\pm(v, u) = K_\pm(v + u, v - u; v_{\max}).$$

The boundary functions F_j $(j = 0, 1, 2)$ are thus transformed into

$$\tilde{F}_j(v, u) := F_j(v + u, v - u) = 1 - \frac{v^2}{a_j^2} - \frac{u^2}{b_j^2}.$$

This transformation reduces the support of the functions $f_\pm$ (the intersection $E_1 \cap E_2$) into $\tilde{E}_1 \cap \tilde{E}_2$ in the vu plane. Assuming the ordering $0 < b_2 < b_1 < 1$ and $0 < a_1 < a_2 < 1$, we observe that $\tilde{E}_1 \cap \tilde{E}_2$ is decomposed into a disjoint union: $\tilde{E}_1 \cap \tilde{E}_2 = \tilde{D}_1 \cup \tilde{D}_2$, where $\tilde{D}_1 = \{(v, u) \mid a < |v| \leqslant a_1,\ |u| \leqslant r_1\}$ and $\tilde{D}_2 = \{(v, u) \mid |v| \leqslant a,\ |u| \leqslant r_2\}$ with $r_j = (b_j/a_j)(a_j^2 - v^2)^{1/2}$ $(j = 1, 2)$. As illustrated in Fig. 5, the fate of these two regions as the 1D limit $b \to 0$ determines the convergence to the Konno function f_{K}.

This argument is justified by the following proposition, which is proved in Appendix B.

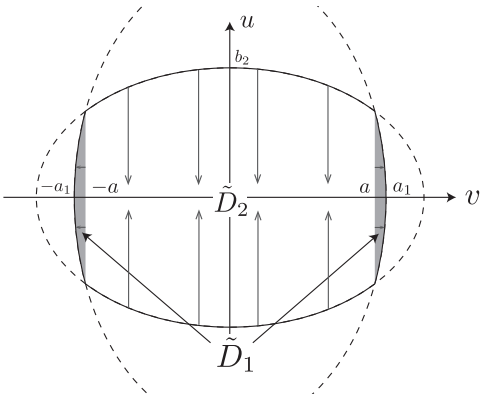


FIG. 5. Domain deformation toward the 1D limit. The support of the 2D Konno functions $f_\pm$ is depicted in the rotated coordinate system (v, u), which is decomposed into $\tilde{D}_1$ and $\tilde{D}_2$. The region $\tilde{D}_1$ collapses to points $(v, u) = (\pm a_1, 0)$, while $\tilde{D}_2$ shrinks to the 1D interval $[-a_1, a_1]$, which coincides with the support of f_{K}.

Proposition 2. Let $(a, b) \in \Delta_{(0,1)}$. For any bounded continuous function $\tilde{h}$, the following holds:

$$\lim_{b\to 0} \iint_{\tilde{D}_1} \tilde{h}\tilde{K}_\pm dv du = 0,$$

$$\lim_{b\to 0} \iint_{\tilde{D}_2} \tilde{h}\tilde{K}_\pm dv du = \frac{\pi b_1}{4} \int_{-a_1}^{a_1} \frac{1-v^2}{\sqrt{a_1^2 - v^2}} \tilde{h}(v, 0)\, dv.$$

We examine the implications of Proposition 2. Indeed, rotating coordinates by $\pi/4$ gives

$$f_\pm(v+u, v-u) = \frac{\tilde{K}_\pm(v, u)}{\pi^2[1-(v+u)^2][1-(v-u)^2]}.$$

Combining this with Proposition 2 provides that $f_\pm\, dv_1 dv_2$ converges to

$$\frac{\pi b_1}{4}\left(\frac{1-v^2}{\sqrt{a_1^2-v^2}} I_{[-a_1,a_1]}(v)\right)\frac{2\delta_0(u)\, dv du}{\pi^2(1-v^2)^2}$$
$$= f_{\mathrm{K}}(v; a_1)\frac{\delta_0(u)\, dv du}{2}$$

in the sense that

$$\lim_{b\to 0} \iint h f_\pm dv_1 dv_2 = \frac{1}{2}\int h(v_1, v_1) f_{\mathrm{K}}(v_1; a_1)\, dv_1$$

for any bounded continuous function $h(v_1, v_2)$.

To the best of our knowledge, this is the first instance in which the 1D Konno function f_{K} has been derived from a higher-dimensional model by taking a suitable limit, solidifying the role of $f_\pm$ as the genuine 2D Konno functions. Note that this argument demonstrates the convergence mechanism for the state-independent part $f_\pm$; the rigorous proof of Theorem 2 for the entire PDF $\rho_{(a,b)}$, which requires the precise definition of the weight functions $w_\pm$ in Sec. V, is provided in Appendix E.

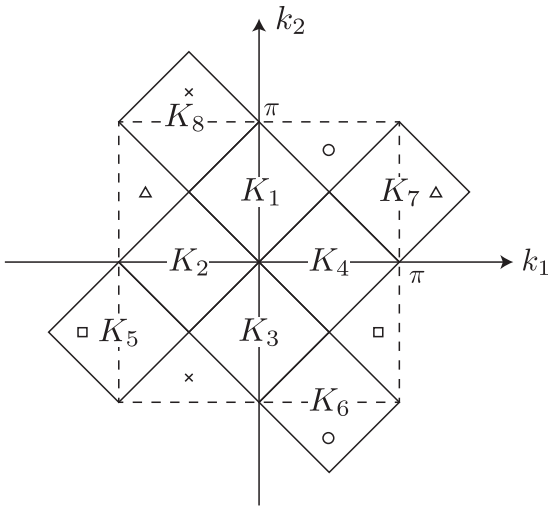


FIG. 6. The "windmill" representation of the wave vector space $\mathbb{T}^2$, partitioned into eight regions K_n $(n = 1, \ldots, 8)$. This structure is a deformation of the standard square domain (indicated by dashed lines), constructed by "cutting and pasting" regions based on the translational invariance of the torus. The symbols illustrate this identification: for example, the △-marked region (top-left of the dashed-line box) is translated by $(+2\pi, 0)$ to form region K_7. Similarly, the ◯-marked region (top-right of the dashed-line box) is translated by $(0, -2\pi)$ to form region K_6. This partition ensures that the signs of s_1 and s_2 by (26) are constant values within each region K_n (see Table IV). All regions include their boundaries, which do not contribute to the integrals.

B. Analytical resolution of singular asymptotics

The explicit derivation of the 2D Konno functions $f_\pm$ offers the first analytical understanding of the singular asymptotics of 2DQWs, a phenomenon previously addressed mainly in geometrical and phenomenological terms [81,86].

While Baryshnikov *et al.* [86] characterized the support of limiting distributions of 2DQWs in terms of the Gaussian curvature of an algebraic variety, neither the explicit boundary of the PDF's support nor the full expression for the PDF had been obtained.

In general, the inverse effective mass tensor is defined by the Hessian matrix $\nabla \otimes \nabla\omega$ of the dispersion relation ω, which is, therefore, equal to the Jacobian matrix $\nabla \boldsymbol{v}$ of the group velocity $\boldsymbol{v} = \nabla\omega$. Consequently, the singularities arise from the infinite effective mass that causes the accumulation of wave packets in the band structure. Ahlbrecht *et al.* [81] demonstrated that for a special 2D2SQW model, the loci, referred to as caustics, where the Jacobian $J(\boldsymbol{k}) = \det(\nabla \boldsymbol{v})$ of the group velocity vanishes, present the boundary of the PDF's domain.

Increasing dimensionality drastically increases the mathematical and physical challenge of noninjectivity. In the 1D case, as seen in the introduction, each velocity $v_\pm$ corresponding to frequencies $\pm\omega$ requires splitting the wave-number space into two domains where $v_\pm$ are injective and have their inverses. The effective mass $m_{\mathrm{eff}} = (d^2\omega/dk^2)^{-1}_{k=0}$, which appeared in (3), is always finite and presents no challenges in the regime $v_{\max} \in (0, 1)$.

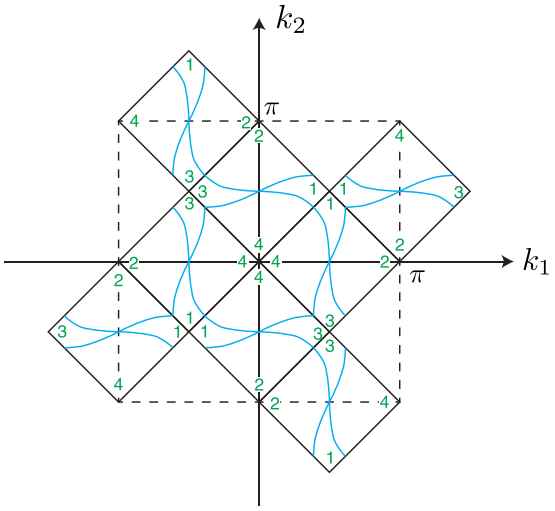


FIG. 7. The finer partition of each region K_n (from Fig. 6) into four subdomains $K_n^{(m)}$ $(m = 1, 2, 3, 4)$. The blue curves defining this separation are the pullbacks onto the k_1k_2 plane of the lines $c_2 = j_\pm c_1$. These lines, which represent the zeros of the quadratic form $\varphi(\boldsymbol{c})$ (i.e., that of the Jacobian), are shown in Fig. 8. The green numerical label m assigned to each subdomain $K_n^{(m)}$ corresponds to the subscript of the region $C^{(m)}$ in Fig. 8.

In contrast, in 2D, the velocity still exhibits two modes, each of which, however, defines a two-variable transformation $(v_{\pm,1}(\boldsymbol{k}), v_{\pm,2}(\boldsymbol{k}))$ from $\mathbb{T}^2$ to $\Sigma(\hat{\boldsymbol{v}}) \subset \mathbb{R}^2$. As will be seen in Sec. V, this transformation partitions the wave-vector space into 64 invertible regions, resulting in 128 combinations for the two modes. This inherent complexity underscores that the partition boundaries are not mere technicalities, but also explicitly represent the caustic loci themselves, where the Jacobian vanishes, and the effective mass diverges.

Our contribution, the successful construction of the inverses of these noninjective maps thus clarifies this universal singular structure of effective-mass divergence. Specifically, the caustic loci displayed as red lines in Ref. [81], [Fig. 4(a)] for a particular 2D2SQW is rigorously derived in our paper for a more general model, appearing as the partitioning curves to define the invertible domain, which are depicted in our Fig. 7 as arccosine curves on a windmill. While Ahlbrecht *et al.* stated that the caustics "could be calculated," their statement relied on numerical demonstration for a specific 2D2SQW model, rather than providing a universal analytical solution. In contrast, our rigorous analysis, built on the intricate algebraic-geometrical partitioning of the wave-vector space, naturally determines the loci of caustics, which precisely corresponds to the boundary of the PDF's domain, or equivalently the joint spectrum $\Sigma(\hat{\boldsymbol{v}})$ of the velocity operators. See Sec. V A for more details.

C. Comparison with other 2D models

1. Generalized Grover walks in 2D

Watabe *et al.* [71] analytically derived the explicit expression of the limit distribution for a 2D four-state QW model, referred to as a generalized Grover walk (GGW), with a generalized four-state Grover coin [83]:

$$C_{\mathrm{G}} = \begin{pmatrix} q\Lambda - 1 & \sqrt{pq}\Lambda \\ \sqrt{pq}\Lambda & p\Lambda - 1 \end{pmatrix} \quad \text{with } \Lambda = \begin{pmatrix} 1 & 1 \\ 1 & 1 \end{pmatrix}, \tag{21}$$

where $p, q \geqslant 0$ and $p + q = 1$. Identifying the Hilbert space $\ell^2(\mathbb{Z}^2; \mathbb{C}^4)$ of states for this model with $\mathcal{H} \oplus \mathcal{H}$ allows us to represent the shift operator S_{G} for this model as $S_{\mathrm{G}} = S_1 \oplus S_2$, where $\mathcal{H}$ and S_j $(j = 1, 2)$ are as defined in Sec. II. Then $U_{\mathrm{G}} = S_{\mathrm{G}}C_{\mathrm{G}}$ defines the evolution operator for the GGW model.

A spectral mapping technique, first elaborated by Szegedy [26] and further developed by several authors [87–90], clarifies the relation between the GGW and our model. To see this, rewriting U_{G} as

$$U_{\mathrm{G}} = [S_{\mathrm{G}}(\sigma_x \oplus \sigma_x)] \times [(\sigma_x \oplus \sigma_x)C_{\mathrm{G}}] =: S'_{\mathrm{G}}C'_{\mathrm{G}}$$

clarifies the chiral symmetry of U_{G}, which stems from the fact that S'_{G} and C'_{G} are unitary involutions, i.e., $a^\dagger = a^{-1} = a$ (and thus $a^2 = 1$). See Ref. [63] for the relation between the chiral symmetry and the spectral mapping technique. Actually, the unitarity and involutivity of S'_{G} follow from the fact that it acts on $\mathcal{H} \oplus \mathcal{H}$ as the direct sum $S'_1 \oplus S'_2$ of unitary involutions. These properties for C'_{G} are clear because one can write

$$C'_{\mathrm{G}} = 1 - 2|\Phi_0\rangle\langle\Phi_0|,$$

where $|\Phi_0\rangle$ is the transpose of $(\sqrt{p}, \sqrt{p}, -\sqrt{q}, -\sqrt{q})/\sqrt{2}$.

Define an operator T_{G} on $\ell^2(\mathbb{Z}^2)$ by

$$T_{\mathrm{G}}\psi = \langle\Phi_0|S'_{\mathrm{G}}(\psi \otimes |\Phi_0\rangle)$$

for any $\psi \in \ell^2(\mathbb{Z}^2)$. This operator, called the discriminant, plays an important role in the spectral mapping technique. As shown in [91], the action of T_G is given by

$$(T_{\mathrm{G}}\psi)(\boldsymbol{x}) = \frac{p}{2}[\psi(\boldsymbol{x} + \boldsymbol{e}_1) + \psi(\boldsymbol{x} - \boldsymbol{e}_1)] + \frac{q}{2}[\psi(\boldsymbol{x} + \boldsymbol{e}_2) + \psi(\boldsymbol{x} - \boldsymbol{e}_2)].$$

The discriminant T_{G} for the GGW is the generator of the 2D continuous-time QW (CTQW) [42] with horizontal and vertical transition probabilities $p/2$ and $q/2$. It is also commonly known as the (free) discrete Schrödinger operator on $\mathbb{Z}^2$. Because T_{G} is translation invariant on $\mathbb{Z}^2$, the Fourier transform diagonalizes T_{G} in the wave-vector space as

$$\hat{T}_{\mathrm{G}}(\boldsymbol{k}) = p\cos k_1 + q\cos k_2, \quad \boldsymbol{k} \in \mathbb{T}^2. \tag{22}$$

The following proposition summarizes the spectral mapping technique, which facilitates the calculation of the spectrum of U_{G}:

Proposition 3 (Spectral mapping). The absolutely continuous part of U_{G} is unitarily equivalent to

$$e^{i\arccos T_{\mathrm{G}}} \oplus e^{-i\arccos T_{\mathrm{G}}}$$

acting on $\mathcal{H} \simeq \ell^2(\mathbb{Z}^2) \oplus \ell^2(\mathbb{Z}^2)$.

Proof. The construction developed in Ref. [89] of the generator for chiral-symmetric unitary operators implies that the absolutely continuous part of U_{G} is unitarily equivalent to $e^{i\arccos T_{\mathrm{G}}} \oplus e^{-i\arccos T_{\mathrm{G}}}$. ∎

This proposition implies that the dispersion relation $\omega_{\mathrm{G}}(\boldsymbol{k})$ of the GGW satisfies $\cos\omega_{\mathrm{G}}(\boldsymbol{k}) = \hat{T}_{\mathrm{G}}(\boldsymbol{k})$ and the absolutely

continuous part of U_{G} can be diagonalized as $e^{i\omega_{\mathrm{G}}(\boldsymbol{k})} \oplus e^{-i\omega_{\mathrm{G}}(\boldsymbol{k})}$.

To relate the GGW and our evolution $U = S_2C_2S_1C_1$, which has been assumed to have the coins $C_j = C(a_j; 0, 0, 0)$ defined in (11), recasting the parameters (p, q) of the GGW as (a, b) requires that $p + q = 1$ if and only if $(a, b) \in \Delta_1$.

Theorem 5. Let $(p, q) \in \Delta_1$. Then, the absolutely continuous part of U_{G} is unitarily equivalent to $U = S_2C_2S_1C_1$ with $C_j = C(\sqrt{p}; 0, 0, 0)$ for $j = 1, 2$.

Proof. As mentioned in the proof of Lemma 4, $(a, b) \in \Delta_1$ if and only if $a_1 = a_2 = \sqrt{a}$. Comparing (13) with (22) and applying the change of variables $\boldsymbol{k}' = (k_1 + k_2, k_2 - k_1 + \pi)$, we obtain the relation

$$\tau(\boldsymbol{k}) = a\cos(k_2 + k_1) + b\cos(k_2 - k_1 + \pi) = T_{\mathrm{G}}(\boldsymbol{k}'),$$

where we have used $(p, q) = (a, b)$ in the last equality. As shown in Sec. V, the Fourier transform diagonalizes our evolution operator U as $e^{i\omega(\boldsymbol{k})} \oplus e^{-i\omega(\boldsymbol{k})}$. The periodicity of $\mathbb{T}^2$ ensures the existence of a unitary transformation between the wave-vector spaces that implements the change of variables $\boldsymbol{k} \mapsto \boldsymbol{k}'$. Therefore, $e^{i\arccos T_{\mathrm{G}}} \oplus e^{-i\arccos T_{\mathrm{G}}} \simeq U$. ∎

The following corollary, a direct consequence of Theorem 5, generalizes the WLT obtained by Watabe *et al.* [71] to general initial states. To emphasize the dependence on (p, q), we use $C_{\mathrm{G}}(p, q)$ to denote the generalized Grover coin C_{G} defined in (21).

Corollary 1. Let $(p, q) \in \Delta_1$ and $\boldsymbol{X}_t^{\mathrm{G}}$ be the position of the GGW with the coin operator $C_{\mathrm{G}}(p, q)$ and the initial state Ψ_0^{G}. Then the limiting distribution of $\boldsymbol{X}_t^{\mathrm{G}}/t$ is represented as

$$[\mu_{\mathrm{G}}\delta_0(v_1, v_2) + w_{\mathrm{G}}(v_1, v_2)f(v_1, v_2)]dv_1dv_2,$$

where the initial state Ψ_0^{G} determines the weight function w_{G} and the non-negative constant μ_{G}.

Proof. The proof follows the standard approach developed in [63,89]. It shows that μ_{G} is the probability $P(V_1 = V_2 = 0)$ that the asymptotic velocity is zero, and it is given by the squared norm of the projection of Ψ_0^{G} to $\ker(U^2 - 1)$. The weight function w_{G} is defined by (46) with the initial state Ψ_0^{G} replaced by the projection of Ψ_0^{G} to $\ker(U^2 - 1)^{\perp}$. ∎

Regarding prior work, Di Franco *et al.* [72] derived a PDF whose support is the interior of E [defined in (6)], while Watabe *et al.* [71] calculated the map's image, identifying this interior and four specific boundary points. Since the joint spectrum $\Sigma(\hat{\boldsymbol{v}})$ must be closed, our analysis completes this picture by taking the closure, confirming $\Sigma(\hat{\boldsymbol{v}})$ is the entire closed ellipse E. Notably, the $\boldsymbol{k} \mapsto \boldsymbol{k}'$ transformation in the proof of Theorem 5 induces a $\pi/4$ rotation; the PDF in Ref. [71] corresponds to our PDF f [defined in (5)] rotated by $\pi/4$.

2. Alternate quantum walks

Our model includes the AQW model [72] with the coin operators

$$C_1 = C_2 = C\left(\cos\gamma; \frac{\pi}{2}, \frac{\pi}{2}, -\pi\right) = \begin{pmatrix} \cos\gamma & \sin\gamma \\ \sin\gamma & -\cos\gamma \end{pmatrix}.$$

In this case, $(a, b) \in \Delta_1$ since $a = \cos^2\gamma$, $b = \sin^2\gamma$, and $a + b = 1$. By choosing the coin operator in this way, all AQWs are represented by our model in the regime Δ_1.

In Ref. [72], Di Franco *et al.* demonstrate the possibility of mimicking the GGW using the alternate QW. More precisely, Ref. [72], Theorem 2] states that for the initial state Ψ_0 with $\Psi_0(\boldsymbol{x}) = \boldsymbol{0}$ except for the origin $\boldsymbol{x} = \boldsymbol{0}$, there exists an initial state of the GGW such that the probability distribution of the position for the AQW coincides with that of the GGW for any time t. Theorem 5 generalizes this fact to any initial state Ψ_0 (even those where $\Psi_0(\boldsymbol{x}) \neq \boldsymbol{0}$ for all $\boldsymbol{x} \neq \boldsymbol{0}$) of the AQW.

We also note the 2D2SQW model presented in Ref. [85], Sec. 5.2], defined by the evolution operator $W(k_1, k_2) = e^{ik_1\sigma_x}e^{ik_2\sigma_z}$ on $\mathbb{T}^2$. Although this model appears different from an AQW, we can show its unitary equivalence. By utilizing the Hadamard matrix H, which diagonalizes σ_x, we find $HW(k_1, k_2)H = e^{ik_1\sigma_z}C_1e^{ik_2\sigma_z}C_2$ with $C_1 = C_2 = H$. Based on Lemma 1, this evolution is unitarily equivalent to our model with coin operators $C_1 = C_2 = C(1/\sqrt{2}; 0, 0, 0)$. This corresponds precisely to the case $a = b = 1/2$, yielding $v_{\max} = a + b = 1$. Consequently, our general result for the Δ_1 regime predicts that the joint spectrum $\Sigma(\hat{\boldsymbol{v}})$—the ellipse E defined in (6)—degenerates into a unit circle for this specific case, consistent with the implications of the analysis in Ref. [85].

The last and present sections imply that Theorem 3 alone recovers the known results for the limit distribution of QWs on the square lattice [71,72]. Notably, Theorem 1, the central finding of this paper, introduces a previously unexplored class of QWs whose limit distributions are explicitly obtained. The 2D Konno functions derived in Theorem 1 are fundamentally different from those found in previous works, offering a fresh perspective for the study of QWs.

3. Generalization to higher dimensions

As detailed in Secs. V A and V B, our analytical success in the 2D case hinges on the ability to represent the velocity map and its Jacobian using independent parameters $c_j = \cos l_j$ $(j = 1, 2)$ with l_j being linear combinations of k_j. This representation facilitates the explicit construction of the inverse velocity map in Secs. V C and V D. The analytical tractability of this process depends on the dispersion relation $\omega(\boldsymbol{k}) = \arccos\tau(\boldsymbol{k})$ with $\tau(\boldsymbol{k}) = ac_1 - bc_2$.

This process is, however, not easily extended to higher dimensions. To clarify the obstacles encountered in such generalizations, it is instructive to compare our case with CTQWs, whose dispersion relation takes the form $\omega(\boldsymbol{k}) = \sum_{j=1}^{d} h_j\cos k_j$. This structure allows for the separation of variables in the time evolution as $e^{-it\omega(\boldsymbol{k})} = \prod_{j=1}^{d}(e^{-ith_j\cos k_j})$. Consequently, the d-dimensional limit distribution factorizes into a product of 1D arcsine laws, much like how the characteristic function in the CLT factorizes to produce a universal Gaussian.

In contrast, the arccos function in our discrete-time counterpart introduces a nonlocality. Much like the square-root operator $\sqrt{-\Delta}$ for a relativistic particle—which corresponds to $(\sum k_j^2)^{1/2}$, in contrast with the local operator $-\Delta \sim \sum k_j^2$ for a nonrelativistic particle—this arccos coupling prevents the separation of variables. Furthermore, the argument of the arccos function is generally given by $\tau(\boldsymbol{k}) = \sum_{j=1}^{2^{d-1}} h_j\cos l_j$, where each l_j is a linear combination of $k_1, \ldots, k_d$. As can be readily verified, the number of these cosine terms grows as 2^{d-1}, quickly exceeding the spatial dimension d.

Unlike CTQWs, where the number of cosine terms always matches d and the variables are separated in the time evolution, the identity $d = 2^{d-1}$ between the spatial dimension and the number of cosines in our discrete-time counterpart is a numerical coincidence limited to $d = 1$ and 2. Beyond these dimensions ($d \geqslant 3$), the loss of this structural alignment and the inherent nonlocality of the arccos function pose a formidable algebraic barrier to the explicit inversion of the velocity map.

V. SKETCH OF PROOFS

This section outlines the proofs for our main results: Theorem 1 (the $v_{\max} < 1$ regime) and Theorem 3 (the $v_{\max} = 1$ regime).

Our analysis is based on the framework of Grimmett *et al.* [37], which defines the limiting PDF via the joint spectral measure $d\langle\Psi_0|E_{\hat{\boldsymbol{v}}}(\boldsymbol{v})\Psi_0\rangle$. The core challenge in 2D is that the group velocity $\boldsymbol{v}_\star : \mathbb{T}^2 \to \Sigma(\hat{\boldsymbol{v}})$ is a highly noninjective map. To derive the PDF, we must analytically perform the change of variables from the wave vector $\boldsymbol{k}$ to the velocity $\boldsymbol{v}$ by rigorously inverting this map.

Our proof proceeds as follows: First, we determine the joint spectrum $\Sigma(\hat{\boldsymbol{v}})$ (the PDF's support). Second, we calculate the Jacobian J of the velocity map, showing its zeros (the caustics) define the support's boundary. Third, we use the Jacobian's sign to partition $\mathbb{T}^2$ into subdomains where the map is invertible. We then explicitly construct the inverse maps $\boldsymbol{k}(\boldsymbol{v})$. Finally, we use these components to transform the spectral measure from $\boldsymbol{k}$ space to $\boldsymbol{v}$ space, yielding the final PDF $\sum_\bullet w_\bullet f_\bullet$.

A. Joint spectrum $\Sigma(\hat{\boldsymbol{v}})$

The translation-invariance property allows us to diagonalize the evolution U into a two-by-two unitary matrix-valued function $\hat{U}(\boldsymbol{k})$ in the wave-vector space $\mathbb{T}^2$ and represent its spectral decomposition as

$$\hat{U} = e^{i\omega}|\omega_+\rangle\langle\omega_+| + e^{-i\omega}|\omega_-\rangle\langle\omega_-|,$$

where $\omega(\boldsymbol{k}) = \arccos\tau(\boldsymbol{k})$ is the dispersion relation with $\tau(\boldsymbol{k})$ defined in (13), and $|\omega_\star(\boldsymbol{k})\rangle$ ($\star = \pm$) forms an ONB of eigenbases for $\boldsymbol{k} = (k_1, k_2) \in \mathbb{T}^2$. The velocity operator $\hat{\boldsymbol{v}}$ in the wave-vector space is given by the vector $\hat{\boldsymbol{v}} = (\hat{v}_1, \hat{v}_2)$ of two-by-two matrices

$$\hat{v}_j = \sum_{\star=\pm} v_{\star,j}|\omega_\star\rangle\langle\omega_\star|, \quad j = 1, 2, \tag{23}$$

where the functions $v_{\pm,j}$ are characterized by the group velocities $\mp\nabla\omega = (v_{\pm,1}, v_{\pm,2})$ corresponding to the modes $|\omega_\pm\rangle$. Note that the group velocity here is defined proportional to $\mp\nabla\omega$, corresponding to the time evolution $e^{\pm i\omega t}$. This sign convention is consistent with the 1D QW literature [42].

To streamline the description, we introduce the following notation for any wave vector $\boldsymbol{k} = (k_1, k_2)$:

$$l_1 := k_2 + k_1, \quad l_2 := k_2 - k_1, \tag{24}$$

$$c_1 := \cos l_1, \quad c_2 := \cos l_2, \tag{25}$$

$$s_1 := \sin l_1, \quad s_2 := \sin l_2, \tag{26}$$

$$v_1 := -\frac{as_1 + bs_2}{\sqrt{1-\tau^2}}, \quad v_2 := -\frac{as_1 - bs_2}{\sqrt{1-\tau^2}}. \tag{27}$$

Here, the functions τ and $v_{\star,j}$ appearing in (23) can be represented, respectively, as $\tau = ac_1 - bc_2$ and

$$v_{\pm,j} = \pm v_j, \quad j = 1, 2. \tag{28}$$

The assertions (i) and (ii) of Proposition 1 are a direct consequence of (27), since $\hat{v}_j$ is the direct sum of the two multiplication operators by the functions $v_{\star,j}$, whose spectrum is given by the union of the ranges of $v_{\star,j}$ ($\star = \pm$) as functions. In case of $(a, b) \in \Delta_1$, it follows from (13) that $\tau(\boldsymbol{k})^2 = 1$ at four points $(0, \pm\pi)$ and $(\pm\pi, 0)$, but (27) can be defined almost everywhere.

We conclude this section by stating the following theorem that clarifies the joint spectrum $\Sigma(\hat{\boldsymbol{v}})$. The idea of the proof can be found in Appendix D.

Theorem 6. The joint spectrum is given by

$$\Sigma(\hat{\boldsymbol{v}}) = \begin{cases} E_1 \cap E_2, & (a, b) \in \Delta_{(0,1)} \\ E, & (a, b) \in \Delta_1, \end{cases}$$

where E and E_j are the ellipses defined in (6) and (15).

B. Jacobians of velocity map

In this section, we calculate the absolute value of the Jacobian for the velocity map $\boldsymbol{v}_\star = (v_{\star,1}, v_{\star,2})$ with $\star = \pm$. As established in Theorem 6, these maps define 2D transformations $\boldsymbol{v}_\star : \mathbb{T}^2 \to \Sigma(\hat{\boldsymbol{v}})$. From (28) and the multilinearity of determinants, the Jacobians of $v_\star$ are identical. We therefore denote this common determinant by J, which can be written as

$$J = \det(\nabla\boldsymbol{v}),$$

with $\boldsymbol{v} = (v_1, v_2)$ defined in (27).

The remainder of this section is devoted to a sketch of the calculation of J and the absolute value of its inverse, $|J|^{-1}$, as functions of $\boldsymbol{v} = (v_1, v_2)$. Since the full derivation is algebraically intensive, we highlight only the principal steps and leave the details to the reader.

1. *Quadratic form $\varphi(\boldsymbol{c})$ for the Jacobian J*

We introduce additional notation that makes calculations more tractable:

$$\tau_\pm := ac_1 \pm bc_2, \quad \sigma_\pm := as_1 \pm bs_2, \tag{29}$$

where c_i, s_i are defined in Eqs. (25) and (26) and we observe that $\tau = \tau_-$. A key advantage of this notation is that it provides compact expressions for the gradients:

$$\nabla\sigma_\pm = (\tau_\mp, \tau_\pm), \quad \nabla\tau_\pm = -(\sigma_\mp, \sigma_\pm).$$

Consequently, the velocity $\boldsymbol{v}$ and its derivative can be expressed solely in terms of $\tau_\pm$ and $\sigma_\pm$. The following proposition, obtained by using such relations, serves as the starting point of our analysis.

Proposition 4. The Jacobian is represented in terms of $\boldsymbol{c} = (c_1, c_2)$ and τ as

$$J = -\frac{4ab\varphi(\boldsymbol{c})}{(1-\tau^2)^2}, \tag{30}$$

where the function φ is a quadratic form given by

$$\varphi(\boldsymbol{c}) = abc_1^2 + (1 - a^2 - b^2)c_1c_2 + abc_2^2. \tag{31}$$

Observe from (30) that the quadratic form φ is of central importance, as its zeros correspond to the vanishing of J. These zeros, therefore, define the boundaries of our domain separation, which physically represent the caustics of the group-velocity map, or equivalently, the locus of the divergent effective mass.

2. *Quadratic equation for* $\mathbf{1 - \tau^2}$

As a result of Proposition 4, the Jacobian J has been expressed in terms of c_i and $1 - \tau^2$. Here, we represent $1 - \tau^2$ in terms of the velocity $\boldsymbol{v}$.

To this end, squaring both sides of (13) provides

$$\tau^2 - a^2c_1^2 - b^2c_2^2 = -2abc_1c_2. \tag{32}$$

Squaring both sides of (32) again, and then substituting [obtained from (27)]

$$c_i^2 = \begin{cases} 1 - (1 - \tau^2)(v_1 + v_2)^2/(4a^2), & i = 1 \\ 1 - (1 - \tau^2)(v_1 - v_2)^2/(4b^2), & i = 2 \end{cases} \tag{33}$$

eliminates the functions c_j^2 and finds that $T := 1 - \tau^2$ satisfies the following quadratic equation:

$$AT^2 - 4abF_0T + B = 0, \tag{34}$$

where F_0 is defined in Eq. (14) and

$$A = \left(1 - v_1^2\right)\left(1 - v_2^2\right),$$
$$B = [1 - (a + b)^2][1 - (a - b)^2].$$

Proposition 5. Let D be the discriminant of the quadratic equation (34). Then

(1) the reduced discriminant $D' := D/4 = (2abF_0)^2 - AB$ is equal to $(2ab)^2F_1F_2$:

$$(2abF_0)^2 - AB = (2ab)^2F_1F_2.$$

(2) the solution $T = 1 - \tau^2$ of the quadratic equation (34) is given by

$$1 - \tau^2 = 2ab\left[\frac{F_0 \pm \sqrt{F_1F_2}}{\left(1 - v_1^2\right)\left(1 - v_2^2\right)}\right]. \tag{35}$$

We omit the proof, but offer some brief remarks:

(1) While (2) follows straightforwardly from (1) by applying the quadratic formula to (34), the verification of statement (1) is far from trivial and involves a tedious algebraic calculation of $(2abF_0)^2 - AB$.

(2) The RHS of (35) is a two-valued function of $\boldsymbol{v}$, an ambiguity that stems from the noninjectivity of $\boldsymbol{v} = \boldsymbol{v}(\boldsymbol{k})$. Resolving this requires choosing a specific branch for the inverse function $\boldsymbol{k}(\boldsymbol{v})$, which is achieved by restricting the domain $\mathbb{T}^2$ to a region where the mapping is injective. The choice of branch determines the sign $\pm$ of the RHS.

3. *Caustics and Jacobian*

For $(a, b) \in \Delta_{(0,1)}$, Propositions 4 and 5 allow us to eliminate c_1 and c_2 from the quadratic form $\varphi(\boldsymbol{c})$ defined in (31) and represent the Jacobian J as a function of v. Actually, Eqs. (32) and (33) eliminate c_1 and c_2, and then, using Eqs. (34) and (35), establishes

$$-2ab\varphi(\boldsymbol{c}) = B - 2abF_0T$$
$$= T(2abF_0 - AT) = \mp 2abT\sqrt{F_1F_2}.$$

Substituting this into the RHS of (30) provides

$$J = \frac{\mp 4ab\sqrt{F_1F_2}}{1 - \tau^2}. \tag{36}$$

Combining this with (35) and taking into consideration the second remark on the sign $\pm$ corresponds to the branches of the inverse function $\boldsymbol{k} = \boldsymbol{k}(\boldsymbol{v})$, we can represent the reciprocal of the Jacobian J in terms of the velocity $\boldsymbol{v} = (v_1, v_2)$ as

$$1/J = \begin{cases} -\pi^2 f_+, & J < 0 \\ +\pi^2 f_-, & J > 0, \end{cases} \tag{37}$$

where the functions $f_\pm$ are the 2D Konno functions defined in (16). For notational simplicity, we write the absolute values of the RHS of (37) as $|J|_{+1}^{-1}$ for $J < 0$ and $|J|_{-1}^{-1}$ for $J > 0$, which are identical, from a standard result in bivariate calculus, with the absolute value of the Jacobian of an inverse function $\boldsymbol{k} = \boldsymbol{k}(\boldsymbol{v})$.

Moreover, combining Theorem 6 with Eqs. (30) and (36) provides that, for $\boldsymbol{k} \in \mathbb{T}^2$ and $\boldsymbol{v} = \boldsymbol{v}_\star(\boldsymbol{k})$, the following are equivalent:

(a) The Jacobian J vanishes, i.e., $J(\boldsymbol{k}) = 0$.

(b) The quadratic form φ has zeros, i.e., $\varphi(\boldsymbol{c}) = 0$.

(c) $\boldsymbol{v}$ lies on $\partial(E_1 \cap E_2)$, i.e., $F_1(\boldsymbol{v})F_2(\boldsymbol{v}) = 0$ and $F_j(\boldsymbol{v}) \geqslant 0$.

(d) $\boldsymbol{v}$ lies on the boundary of $\Sigma(\hat{\boldsymbol{v}})$, i.e., $\boldsymbol{v} \in \partial\Sigma(\hat{\boldsymbol{v}})$.

For $(a, b) \in \Delta_1$ that is equivalent to that of $B = 0$, Proposition 5 dictates

$$1 - \tau^2 = 0 \text{ or } \frac{4abF_0}{\left(1 - v_1^2\right)\left(1 - v_2^2\right)}.$$

However, the former situation $1 - \tau^2 = 0$ happens only at one of the four points $\boldsymbol{k} = (\pm\pi, 0),\ (0, \pm\pi)$, where $\tau(\boldsymbol{k})^2 = 1$. Otherwise, an argument similar to that above provides $-2ab\varphi(\boldsymbol{c}) = -2abF_0T$. Substituting this into (30), we obtain $|J|^{-1} = \pi^2 f$, where the function f is defined in (5) and $|J|^{-1}$ simply denotes the reciprocal of $|J|$, since no branch exists for this case.

In summary, we arrive at the following:

Theorem 7 (Reciprocal of Jacobian). Let $\mathrm{Sing}(J)$ be the singular set of the velocity map, i.e., the zeros of the Jacobian: $\mathrm{Sing}(J) = \{\boldsymbol{k} \in \mathbb{T}^2 \mid J(\boldsymbol{k}) = 0\}$.

(1) Let $(a, b) \in \Delta_{(0,1)}$. Then $|J|_{\pm 1}^{-1} = \pi^2 f_\pm$. The limit PDF forms a caustic, diverging on the image of the singular set, which coincides with the boundary of the support: $\boldsymbol{v}(\mathrm{Sing}(J)) = \partial\Sigma(\hat{\boldsymbol{v}})$.

(2) Let $(a, b) \in \Delta_1$. Then $|J|^{-1} = \pi^2 f$. The limit PDF diverges on the image of the singular set, which, in this case, is the discrete four-point set: $\boldsymbol{v}(\mathrm{Sing}(J)) = \{\pm(1, a - b), \pm(a - b, 1)\}$.

C. Domain separations

The separation of the domain for the velocity map $\boldsymbol{v} = \boldsymbol{v}_\star(\boldsymbol{k})$, required to properly define its inverse, is not merely a

TABLE IV. Signs of s_1 and s_2.

n	$\mathrm{sgn}(s_1)$	$\mathrm{sgn}(s_2)$
1, 5	+1	+1
2, 6	−1	+1
3, 7	−1	−1
4, 8	+1	−1

technical procedure. It is fundamentally the problem of identifying the physical region of finite effective mass, distinct from the caustics where it diverges. To implement this separation, we proceed in several steps.

1. Separating windmill to eight domains K_n

The periodicity of the wave-vector space $\mathbb{T}^2$ allows us to identify it with a "windmill-like" region, which we then partition it into eight coarse domains K_n $(n = 1, 2, \ldots, 8)$, as shown in Fig. 6. Within the windmill-like domain, the boundaries of each domain K_n are parallel to the rotated coordinate axes l_1 and l_2 [defined in (24)]. This alignment uniquely determines the signs of s_i $(i = 1, 2)$ in each region K_n, as indicated in Table IV.

2. Partition K_n into four subdomains $K_n^{(m)}$

In order that the restrictions $\boldsymbol{v}_\star|_{K_n^{(m)}}$ of the velocity map are invertible, we further partition K_n into four subdomains, $K_n^{(m)}$ $(m = 1, 2, 3, 4)$, which are illustrated in Fig. 7. The key to define such a finer separation is mapping each region K_n onto the square region $[-1, 1]^2$ in the c_1c_2 plane and defining the separation in the c_1c_2 plane. This allow us to avoid the noninjectivity originating from the trigonometric functions c_i and s_i. Then the quadratic form $\varphi(\boldsymbol{c})$ successfully determines the sign of the Jacobian J in the c_1c_2 plane as stated in the following proposition (we give the proof in Appendix C):

Proposition 5 (branches of Jacobian). The sign of the Jacobian J is determined by the zeros of the quadratic form $\varphi(\boldsymbol{c})$ [defined in Eq. (31)]. These zeros form lines $c_2 = j_\pm c_1$ that partition the c_1c_2 plane into regions $C^{(m)}$, as depicted in Fig. 8. The specific partitioning depends on the parameter regime:

(1) *In the $\Delta_{(0,1)}$ regime*. There exist unique real constants $j_\pm$ satisfying $j_- = 1/j_+$ and $-1 < j_+ < 0$. These lines divide the square $[-1, 1]^2$ into four regions $C^{(m)}$ $(m = 1, 2, 3, 4)$. On each region $C^{(m)}$ (excluding the boundary), the reciprocal of the Jacobian takes a specific branch: $|J|^{-1} = |J|^{-1}_{(-1)^m}$.

(2) *In the Δ_1 regime*. This regime corresponds to the degenerate case $j_+ = j_- = -1$. The line $c_2 = -c_1$ divides the square $[-1, 1]^2$ into two nonempty regions $C^{(m)}$ $(m = 2, 4)$. On these regions (excluding the boundary), the reciprocal of the Jacobian is $|J|^{-1} = |J|^{-1}_{+1}$.

Mapping $C^{(m)}$ back to the original wave-vector space (see Table V for the construction) provides the desired separations $K_n^{(m)}$ as illustrated on the windmill in Fig. 7. The boundaries separating these subdomains $K_n^{(m)}$ are the caustics stated in (1) of Theorem 7.

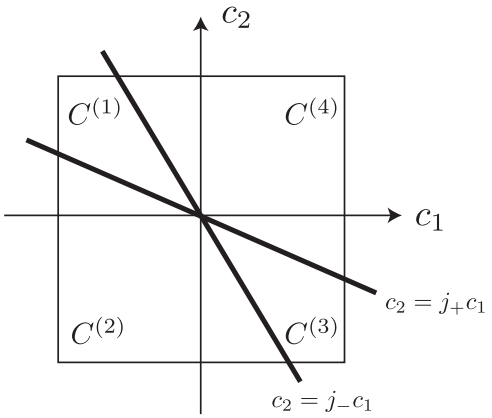


FIG. 8. The separation of the c_1c_2 plane into the four regions $C^{(m)}$ $(m = 1, 2, 3, 4)$ by the lines $c_2 = j_\pm c_1$. These regions correspond to the subdomains $K_n^{(m)}$ shown in Fig. 7. The constants $j_\pm$ are slopes that satisfy the inequalities $j_- < -1 < j_+ < 0$. The degenerate case $j_+ = j_- = -1$ occurs if and only if $v_{\max} = 1$. In this case, the regions $C^{(1)}$ and $C^{(3)}$ collapse.

3. Decomposing $K_n^{(m)}$ into four parts $K_{n,n'}^{(m)}$

In Sec. V C 2, we successfully determined the invertible domains of the velocity map $\boldsymbol{v} = \boldsymbol{v}_\star$ $(\star = \pm)$. In our construction, the Jacobian of $\boldsymbol{v}_\star$ has the same sign on each subdomain $K_n^{(m)}$. The inverse function theorem then states that the restriction $\boldsymbol{v}_\star|_{K_n^{(m)}}$ is injective and therefore invertible.

However, establishing invertibility is not sufficient. To obtain the closed form of the limiting PDF, we must determine $\mathrm{sgn}c_i$, since $v_{\star,j}$ and $|\omega_\star\rangle$ depend not only on s_i but also on c_i. This demands a further separation of each subdomain $K_n^{(m)}$. Fortunately, this task is not complicated. We can again leverage the c_1c_2 plane, where the signs of c_i are naturally determined. In fact, each n'th quadrant $n' = 1, 2, 3, 4$ of this plane corresponds to unique set of signs $(\mathrm{sgn}(c_1), \mathrm{sgn}(c_2))$, as summarized in Table VI.

We thus define a new, finer partition $K_{n,n'}^{(m)}$ by taking the intersection of $C^{(m)}$ and the n'th quadrant in the c_1c_2 plane, and pulling this intersection back to the corresponding domain $K_n^{(m)}$. Although quadrants are typically defined as open sets (excluding the coordinate axes), we explicitly take the closure of their intersection with $C^{(m)}$. This procedure ensures that the boundaries are properly included in the pullback.

TABLE V. Inverse function $\boldsymbol{l} = \boldsymbol{l}(\boldsymbol{c})$.

n	$\boldsymbol{l} = \boldsymbol{l}(\boldsymbol{c})$	n	$\boldsymbol{l} = \boldsymbol{l}(\boldsymbol{c})$
1	$\begin{pmatrix} l_1 \\ l_2 \end{pmatrix} = \begin{pmatrix} \mathrm{Arccos}c_1 \\ \mathrm{Arccos}c_2 \end{pmatrix}$	5	$\begin{pmatrix} l_1 \\ l_2 \end{pmatrix} = \begin{pmatrix} \mathrm{Arccos}c_1 - 2\pi \\ \mathrm{Arccos}c_2 \end{pmatrix}$
2	$\begin{pmatrix} l_1 \\ l_2 \end{pmatrix} = \begin{pmatrix} -\mathrm{Arccos}c_1 \\ \mathrm{Arccos}c_2 \end{pmatrix}$	6	$\begin{pmatrix} l_1 \\ l_2 \end{pmatrix} = \begin{pmatrix} -\mathrm{Arccos}c_1 \\ \mathrm{Arccos}c_2 - 2\pi \end{pmatrix}$
3	$\begin{pmatrix} l_1 \\ l_2 \end{pmatrix} = \begin{pmatrix} -\mathrm{Arccos}c_1 \\ -\mathrm{Arccos}c_2 \end{pmatrix}$	7	$\begin{pmatrix} l_1 \\ l_2 \end{pmatrix} = \begin{pmatrix} -\mathrm{Arccos}c_1 + 2\pi \\ -\mathrm{Arccos}c_2 \end{pmatrix}$
4	$\begin{pmatrix} l_1 \\ l_2 \end{pmatrix} = \begin{pmatrix} \mathrm{Arccos}c_1 \\ -\mathrm{Arccos}c_2 \end{pmatrix}$	8	$\begin{pmatrix} l_1 \\ l_2 \end{pmatrix} = \begin{pmatrix} \mathrm{Arccos}c_1 \\ -\mathrm{Arccos}c_2 + 2\pi \end{pmatrix}$

TABLE VI. Signs of c_1 and c_2.

n'	$\mathrm{sgn}(c_1)$	$\mathrm{sgn}(c_2)$
1	$+1$	$+1$
2	-1	$+1$
3	-1	-1
4	$+1$	-1

Note that for certain combinations of n' and m, this intersection in the c_1c_2 plane may be empty [e.g., $(n', m) = (1, 1)$ suggested by Fig. 8]. In such cases, the corresponding $K^{(m)}_{n,n'}$ is simply considered to be the empty set. Table VII provides a complete classification, summarizing which subdomains $K^{(m)}_{n,n'}$ are nonempty and which are empty ($\emptyset$).With this final partition, the signs of c_i are uniquely fixed within each nonempty subdomain $K^{(m)}_{n,n'}$ (excluding the boundary). As summarized in Table VII, whether a given subdomain is empty depends by construction only on the combination of n' (determining $\mathrm{sgn}c_i$) and m (corresponding to the Jacobian's sign), and not on the coarse index n (determining $\mathrm{sgn}(s_i)$).

This partition is now complete, and the set of all nonempty subdomains $K^{(m)}_{n,n'}$ collectively covers the entire wave-vector space $\mathbb{T}^2$ (identical to the windmill region). Consequently, their images under the velocity map v fully cover the joint spectrum $\Sigma(\hat{\boldsymbol{v}})$. More precisely, as the geometric arrangement of the velocity map and Table VII show, the union of the images $\boldsymbol{v}(K^{(m)}_{n,n'})$ for a single index m (corresponding to a specific Jacobian sign) already covers the entire spectrum:

Theorem 8 [Multicovers of $\Sigma(\hat{\boldsymbol{v}})$]. For each $m = 1, 2, 3, 4$, the joint spectrum $\Sigma(\hat{\boldsymbol{v}})$ can be decomposed into the following unions, where the images $\boldsymbol{v}(K^{(m)}_{n,n'})$ are mutually disjoint, excluding their boundary:

(1) $\bigcup_{n=1,2,3,4} \boldsymbol{v}(K^{(1)}_{n,2}) = \bigcup_{n=5,6,7,8} \boldsymbol{v}(K^{(1)}_{n,2}) = \Sigma(\hat{\boldsymbol{v}})$.

(2) $\bigcup_{\substack{n=1,2,3,4\\ n'=2,3,4}} \boldsymbol{v}(K^{(2)}_{n,n'}) = \bigcup_{\substack{n=5,6,7,8\\ n'=2,3,4}} \boldsymbol{v}(K^{(2)}_{n,n'}) = \Sigma(\hat{\boldsymbol{v}})$.

(3) $\bigcup_{n=1,2,3,4} \boldsymbol{v}(K^{(3)}_{n,4}) = \bigcup_{n=5,6,7,8} \boldsymbol{v}(K^{(3)}_{n,4}) = \Sigma(\hat{\boldsymbol{v}})$.

(4) $\bigcup_{\substack{n=1,2,3,4\\ n'=1,2,4}} \boldsymbol{v}(K^{(4)}_{n,n'}) = \bigcup_{\substack{n=5,6,7,8\\ n'=1,2,4}} \boldsymbol{v}(K^{(4)}_{n,n'}) = \Sigma(\hat{\boldsymbol{v}})$.

This multicovered structure of the joint spectrum is the essential geometric feature that allows for the decomposition of the limiting PDF.

TABLE VII. Classification of subdomains $K^{(m)}_{n,n'}$ as empty ($\emptyset$) or nonempty. The index n' corresponds to the quadrant in the c_1c_2 plane, and m corresponds to the sign of the Jacobian.

	$m = 1$	$m = 2$	$m = 3$	$m = 4$
$n' = 1$	$\emptyset$	$\emptyset$	$\emptyset$	$K^{(4)}_{n,1}$
$n' = 2$	$K^{(1)}_{n,2}$	$K^{(2)}_{n,2}$	$\emptyset$	$K^{(4)}_{n,2}$
$n' = 3$	$\emptyset$	$K^{(2)}_{n,3}$	$\emptyset$	$\emptyset$
$n' = 4$	$\emptyset$	$K^{(2)}_{n,4}$	$K^{(3)}_{n,4}$	$K^{(4)}_{n,4}$

We omit a formal proof, but the key insight is as follows: The union of domains for $n \in \{1, 2, 3, 4\}$ (or, alternatively, $n \in \{5, 6, 7, 8\}$) covers all four sign combinations of (s_1, s_2) (Table IV). Since the $\pi/4$-rotated velocity map $\tilde{v}$ maps the (s_1, s_2) space to the joint spectrum $\Sigma(\hat{\boldsymbol{v}})$ (which is the elliptic intersection $\tilde{E}_1 \cap \tilde{E}_2$ as seen in Sec. IV A), we need only verify the mapping [given by (27)] from the first quadrant, $(|s_1|, |s_2|)$, to the first quadrant of $\Sigma(\hat{\boldsymbol{v}})$, for each m. This is confirmed by showing that the boundaries of the domain $C^{(m)}$ map precisely onto the boundaries of the spectrum. For instance, for $m = 1$, the boundaries $c_2 = j_{\pm}c_1$ (see Fig. 8) map to the elliptic arcs of $\partial\Sigma(\hat{\boldsymbol{v}})$, while the boundaries $c_i = \pm 1$ (implying $s_j = 0$ and thus $\tilde{v}_j = 0$) map to the $\tilde{v}$ axes.

D. Inverse velocity maps

We are now ready to construct the inverse velocity map $\boldsymbol{k} = \boldsymbol{k}(\boldsymbol{v})$. We first consider the case of $(a, b) \in \Delta_{(0,1)}$. The starting point is Eqs. (33) and (35), which together express $|c_i|$ as a function of $\boldsymbol{v} = (v_1, v_2)$:

$$|c_1| = \left[1 - \frac{b(v_1 + v_2)^2(F_0 + (-1)^m\sqrt{F_1F_2})}{2a(1 - v_1^2)(1 - v_2^2)}\right]^{1/2}, \tag{38}$$

$$|c_2| = \left[1 - \frac{a(v_1 - v_2)^2(F_0 + (-1)^m\sqrt{F_1F_2})}{2b(1 - v_1^2)(1 - v_2^2)}\right]^{1/2}, \tag{39}$$

where the sign $(-1)^m$ in the RHS of the above equations corresponds to the branch of $1 - \tau^2$ in Eq. (35) that is identical to the branch $|J|_{(-1)^m}$ for the Jacobian, as seen in Sec. V C. Our task is to construct the explicit inverse $\boldsymbol{k} = \boldsymbol{k}(\boldsymbol{v})$ for each of the "covers" of the joint spectrum $\Sigma(\hat{\boldsymbol{v}})$ established in Theorem 8.

We illustrate this procedure for an arbitrary point $\boldsymbol{v}$ belonging to one of the disjoint images. Assume $\boldsymbol{v}$ lies in the interior of $\boldsymbol{v}(K^{(1)}_{3,2})$, which corresponds to the first decomposition ($n \in \{1, 2, 3, 4\}$) in Theorem 8(1). We can safely ignore the boundaries, as they do not contribute to the final integral.

The multi-index $(n, n', m) = (3, 2, 1)$ provides all the information required to uniquely invert the map:

(1) The index $m = 1$ specifies the correct branch for Eqs. (38)–(39), which corresponds to the sign $(-1)^1 = -1$ in the numerators of the RHS.

(2) The index $n' = 2$ determines the signs of c_i via Table VI as $(\mathrm{sgn}(c_1), \mathrm{sgn}(c_2)) = (-1, +1)$.

Combining these, $\boldsymbol{c}(\boldsymbol{v}) = (c_1(\boldsymbol{v}), c_2(\boldsymbol{v}))$ is uniquely determined as a function of $\boldsymbol{v}$:

$$c_1(\boldsymbol{v}) = -\left[1 - \frac{b(v_1 + v_2)^2(F_0 - \sqrt{F_1F_2})}{2a(1 - v_1^2)(1 - v_2^2)}\right]^{1/2},$$

$$c_2(\boldsymbol{v}) = +\left[1 - \frac{a(v_1 - v_2)^2(F_0 - \sqrt{F_1F_2})}{2b(1 - v_1^2)(1 - v_2^2)}\right]^{1/2}.$$

Finally, the index $n = 3$ selects the unique inverse branch $\boldsymbol{l} = \boldsymbol{l}(\boldsymbol{c})$ from Table V. For $n = 3$, this is $(l_1, l_2) = (-\mathrm{Arccos}c_1, -\mathrm{Arccos}c_2)$. From Eq. (24), the inverse map $\boldsymbol{k} = \boldsymbol{k}(\boldsymbol{v})$ for $\boldsymbol{v} \in \boldsymbol{v}(K^{(1)}_{3,2})$ is thus explicitly given by

$$\boldsymbol{k}(\boldsymbol{v}) = \frac{1}{2}\begin{pmatrix} 1 & -1 \\ 1 & 1 \end{pmatrix}\begin{pmatrix} -\mathrm{Arccos}c_1(\boldsymbol{v}) \\ -\mathrm{Arccos}c_2(\boldsymbol{v}) \end{pmatrix}.$$

This procedure can be applied similarly to all other nonempty subdomains $K^{(m)}_{n,n'}$.

We next consider the case of $(a, b) \in \Delta_1$. The procedure is simpler, as this regime corresponds to the degenerate case $j_+ = j_- = -1$ (see Fig. 8). Consequently, the domains $C^{(1)}$ and $C^{(3)}$ collapse to measure zero, and we only need to consider the $m = 2$ and $m = 4$ branches. Lemma 4 states that in this regime, $F_0 = F_1 = F_2 = F$. This significantly simplifies the expressions for $|c_i|$ in Eqs. (38) and (39). The inverse map $\boldsymbol{k}(\boldsymbol{v})$ is then constructed similarly, but only for the nonempty domains $K^{(2)}_{n,n'}$ and $K^{(4)}_{n,n'}$, which correspond to the single 2D function f defined in (5).

E. Derivation of the limiting PDF

We now arrive at the final step: the derivation of the limiting PDF, $\rho(\boldsymbol{v})$. As established in Sec. III, our goal is to find the density $\rho(\boldsymbol{v})$ of the joint spectral measure $\langle\Psi_0|E_{\hat{\boldsymbol{v}}}(\boldsymbol{v})\Psi_0\rangle$ for the velocity operator associated with the initial state Ψ_0. As mentioned in Sec. III, the function ρ is formally represented as $\rho(\boldsymbol{v}) = |\langle v_1, v_2|\Psi_0\rangle|^2$.

The standard method to identify this density $\rho(\boldsymbol{v})$ is to require that the following equality holds for any bounded continuous function $g(\boldsymbol{v}) = g(v_1, v_2)$:

$$\int_{\Sigma(\hat{\boldsymbol{v}})} g(\boldsymbol{v})\rho(\boldsymbol{v})\,d\boldsymbol{v} = \int_{\Sigma(\hat{\boldsymbol{v}})} g(\boldsymbol{v})\,d\langle\Psi_0|E_{\hat{\boldsymbol{v}}}(\boldsymbol{v})\Psi_0\rangle. \tag{40}$$

Moving the integral to the wave-vector space (via the Fourier transform), in which the velocity operator $\hat{\boldsymbol{v}}$ is diagonal, yields

$$\begin{aligned}(40) &= \sum_{\star=\pm}\int_{\mathbb{T}^2} g(\boldsymbol{v}_\star(\boldsymbol{k}))P_\star(\boldsymbol{k})\frac{d\boldsymbol{k}}{(2\pi)^2}\\ &= \sum_{\star=\pm}\sum_{n,n',m}\int_{K^{(m)}_{n,n'}} g(\boldsymbol{v}_\star(\boldsymbol{k}))P_\star(\boldsymbol{k})\frac{d\boldsymbol{k}}{(2\pi)^2},\end{aligned}$$

where we have set

$$P_\star(\boldsymbol{k}) := |\langle\omega_\star(\boldsymbol{k})|\hat{\Psi}_0(\boldsymbol{k})\rangle|^2,$$

using the eigenstates $|\omega_\star(\boldsymbol{k})\rangle$ and group velocities $\boldsymbol{v}_\star(\boldsymbol{k})$ defined in Sec. V A.

Our strategy is to transform the $\boldsymbol{k}$-space integral on the final line of Eq. (40) back into a $\boldsymbol{v}$-space integral over the joint spectrum $\Sigma(\hat{\boldsymbol{v}})$; the resulting *weight* function that multiplies $g(\boldsymbol{v})$ must then be our PDF, $\rho(\boldsymbol{v})$. This change of variable is precisely what our preparatory work in Secs. V B–V D was for.

To implement our strategy, we must express $P_\star(\boldsymbol{k})$ as a function of $\boldsymbol{v}$ using the inverse velocity maps $\boldsymbol{k} = \boldsymbol{k}(\boldsymbol{v})$ constructed in Sec. V D. This motivates us to introduce a simplified index $\Lambda = (\mu, \nu, \xi) \in \{0, 1\}^3$, whose components are defined to specify one of the eight covers from Theorem 8:

(1) The index $\mu \in \{0, 1\}$ specifies the group of covers, corresponding to the left-han side (LHS) and RHS of the equations in Theorem 8. We define the corresponding n-index set as $N_\mu = \{n + 4\mu \mid n = 1, 2, 3, 4\}$.

(2) The indices $(\nu, \xi) \in \{0, 1\}^2$ specify the original index m, which determines the sign of the Jacobian (Proposition 6). As ν is an auxiliary index, we align the parity of m with ξ so that $J^{-1}_{(-1)^m} = J^{-1}_{(-1)^\xi}$. This mapping is given by

$$m = 2(\nu + 1) - \xi. \tag{41}$$

Each index Λ thus uniquely specifies a k-space domain $K_\Lambda = \bigcup_{n\in N_\mu}\bigcup_{n'} K^{(m)}_{n,n'}$, where m is from (41) and the n' union is over the nonempty domains in Table VII. The inverse map associated with this domain is

$$\boldsymbol{k}_\Lambda(\boldsymbol{v}) := (\boldsymbol{v}|_{K_\Lambda})^{-1}(\boldsymbol{v}) \text{ on } \Sigma(\hat{\boldsymbol{v}}) = \boldsymbol{v}(K_\Lambda).$$

Apply the change of variables $\boldsymbol{k} \mapsto \boldsymbol{v}$ using these inverse maps $\boldsymbol{k} = \boldsymbol{k}_\Lambda(\boldsymbol{v})$ and the corresponding Jacobian (Proposition 6), $d\boldsymbol{k} = |J|^{-1}_{(-1)^\xi} d\boldsymbol{v}$, we can calculate the $P_+(\boldsymbol{k})$ term in Eq. (40):

$$\begin{aligned}&\sum_\Lambda\int_{K_\Lambda} g(\boldsymbol{v}_+(\boldsymbol{k}))P_+(\boldsymbol{k})\frac{d\boldsymbol{k}}{(2\pi)^2}\\ &\quad= \sum_\Lambda\int_{\Sigma(\hat{\boldsymbol{v}})} g(\boldsymbol{v})P_+(\boldsymbol{k}_\Lambda(\boldsymbol{v}))|J|^{-1}_{(-1)^\xi}\frac{d\boldsymbol{v}}{(2\pi)^2}\\ &\quad= \int_{\Sigma(\hat{\boldsymbol{v}})} g(\boldsymbol{v})\left[\sum_\Lambda P_+(\boldsymbol{k}_\Lambda(\boldsymbol{v}))f_{(-1)^\xi}(\boldsymbol{v})\right]\frac{d\boldsymbol{v}}{4}.\end{aligned} \tag{42}$$

To evaluate the $P_-(\boldsymbol{k})$ term, we must perform an additional change of variables $\boldsymbol{v} \mapsto -\boldsymbol{v}$. This transformation is facilitated by the symmetries of the velocity map and the windmill integration domains, as detailed below.

First, Eqs. (27) and (28) provide $\boldsymbol{v}_-(\boldsymbol{k}) = -\boldsymbol{v}(\boldsymbol{k})$. Moreover, the $\boldsymbol{v} \mapsto -\boldsymbol{v}$ transformation in the velocity space (which maps $g(-\boldsymbol{v}) \to g(\boldsymbol{v})$) corresponds to a $\boldsymbol{k} \mapsto -\boldsymbol{k}$ transformation in the wave-vector space.

Next, we see from the windmill structure in Figs. 6 and 7 that the $\boldsymbol{k} \mapsto -\boldsymbol{k}$ map corresponds to a π rotation. This rotation permutes the integral domains $K^{(m)}_{n,n'}$ according to the permutation $\varepsilon = (13)(24)(57)(68) \in S_8$ on the index n. Specifically, the index is transformed as $n \to n + 2$ for $n \in \{1, 2, 5, 6\}$ and $n \to n - 2$ for $n \in \{3, 4, 7, 8\}$, leaving the set of domains as a whole unchanged Moreover, Table IV and (27) show that the permutation ε makes the sign of $\boldsymbol{v}$ opposite; the change of variable $\boldsymbol{v} \mapsto -\boldsymbol{v}$ leaves $P_-(\boldsymbol{k}_\Lambda(\boldsymbol{v}))$ invariant.

Applying these observations for calculating the $P_-(\boldsymbol{k})$ terms in Eq. (40) yields

$$\begin{aligned}&\sum_\Lambda\int_{K_\Lambda} g(\boldsymbol{v}_-(\boldsymbol{k}))P_-(\boldsymbol{k})\frac{d\boldsymbol{k}}{(2\pi)^2}\\ &\quad= \sum_\Lambda\int_{\Sigma(\hat{\boldsymbol{v}})} g(-\boldsymbol{v})P_-(\boldsymbol{k}_\Lambda(\boldsymbol{v}))|J|^{-1}_{(-1)^\xi}(\boldsymbol{v})\frac{d\boldsymbol{v}}{(2\pi)^2}\\ &\quad= \int_{\Sigma(\hat{\boldsymbol{v}})} g(\boldsymbol{v})\left[\sum_\Lambda P_-(\boldsymbol{k}_\Lambda(\boldsymbol{v}))f_{(-1)^\xi}(\boldsymbol{v})\right]\frac{d\boldsymbol{v}}{4}.\end{aligned} \tag{43}$$

We now introduce functions that incorporate the results from Eqs. (42) and (43). To streamline the notation, we relabel our eight inverse map k_Λ with $\Lambda = (\mu, \nu, \xi)$ by setting $\lambda = (\mu, \nu)$ and letting the index ξ correspond to a new index $\bullet = \pm$. We define $\boldsymbol{k}^\bullet_\lambda = \boldsymbol{k}^\bullet_\lambda(\boldsymbol{v})$ as

$$\boldsymbol{k}^\bullet_\lambda = \begin{cases}\boldsymbol{k}^+_\lambda, & \xi = 0\\ \boldsymbol{k}^-_\lambda, & \xi = 1.\end{cases} \tag{44}$$

TABLE VIII. Difference between $v_{\max} < 1$ and $v_{\max} = 1$.

	$v_{\max} < 1$	$v_{\max} = 1$
τ	$\max\|\tau\| < 1$	$\max\|\tau\| = 1$
$\frac{\partial}{\partial k_j}\|\omega_\star(\boldsymbol{k})\rangle$	Bounded	Unbounded
$v_j(\boldsymbol{k})$	Differentiable	Differentiable without four points
$j_\pm$	$j_- < -1 < j_+$	$j_- = j_+ = -1$
F_j	$F_1 \neq F_2$	$F_1 = F_2 = F_0$

With this notation, for $\star, \bullet \in \{+, -\}$, we define the four weight functions $w_{\star\bullet}$ as the sum over the first two indices:

$$w_{\star\bullet}(\boldsymbol{v}) = \sum_{\lambda\in\{0,1\}^2} P_\star(\boldsymbol{k}^\bullet_\lambda(\boldsymbol{v})).$$

Adding Eqs. (42) and (43) and using the above notation provides the following:

$$\begin{aligned}(40) &= \int_{\Sigma(\hat{\boldsymbol{v}})} g(\boldsymbol{v}) \sum_{\star=\pm}\sum_{\bullet=\pm} w_{\star\bullet}(\boldsymbol{v}) f_\bullet(\boldsymbol{v}) d\boldsymbol{v} \\ &= \int_{\Sigma(\hat{\boldsymbol{v}})} g(\boldsymbol{v}) \sum_{\bullet=\pm} w_\bullet(\boldsymbol{v}) f_\bullet(\boldsymbol{v}) d\boldsymbol{v}, \end{aligned} \tag{45}$$

where

$$w_\bullet(\boldsymbol{v}) := \sum_{\star=\pm} w_{\star\bullet}(\boldsymbol{v}) = \sum_{\star=\pm}\sum_{\lambda\in\{0,1\}^2} P_\star(\boldsymbol{k}^\bullet_\lambda(\boldsymbol{v})). \tag{46}$$

This concludes the proof of Theorem 1.

Finally, we address the case $(a, b) \in \Delta_1$. As established in Proposition 6(2), this regime is degenerate: the domains $C^{(1)}$ and $C^{(3)}$ collapse onto the line $c_2 = -c_1$ (see Fig. 8), whose contribution to the integral vanishes, leaving only the domains $C^{(2)}$ and $C^{(4)}$. According to our indexing (41), these domains $C^{(m)}$ $(m = 2, 4)$ correspond to the index $\xi = 0$. From the definitions in (44)–(46), $\xi = 0$ selects only the $\bullet = +$ branch. Therefore, the f_- and w_- contributions vanish entirely. The limiting PDF in Eq. (45) thus simplifies to $\rho(\boldsymbol{v}) = w_+(\boldsymbol{v}) f_+(\boldsymbol{v})$. Lemma 4 shows $f_+(\boldsymbol{v}) = f(\boldsymbol{v})$ for $v_{\max} = 1$, which completes the proof of Theorem 3.

Table VIII summarizes the differences between $v_{\max} < 1$ and $v_{\max} = 1$.

We add one technical remark. Our proof derives the form of the limiting PDF, assuming the existence of the WLT. A standard sufficient condition for the WLT—the boundedness of the eigenstate derivatives—is satisfied for $v_{\max} < 1$ $(\Delta_{(0,1)})$ but fails for $v_{\max} = 1$ (Δ_1). This failure occurs because the derivatives diverge at the four points where $|\tau(\boldsymbol{k})| = 1$. Nevertheless, the WLT itself is known to hold even in this degenerate case [37], Technical remark at the end of Sec. III]. Our derivation of the PDF via integral transformation is therefore justified for all regimes discussed.

VI. CONCLUSION

In this work, we have derived the first exact representation of the limiting PDF for the WLT of a general 2D2SQW by introducing the notion of maximal speed $(v_{\max})$ to classify the dynamics.

Our central achievement is the discovery of 2D Konno functions, $f_\pm$ for the previously unexplored regime $\Delta_{(0,1)}$ [i.e., $v_{\max} \in (0, 1)$], which we establish as the proper 2D generalization of the 1D Konno function f_{K} by demonstrating their convergence to f_{K} in the appropriate 1D limit. Furthermore, our formulation naturally recovers the previously known function f for the Δ_1 regime, where $v_{\max} = 1$ is a degenerate case.

We also derive the closed-form expression for weight functions $w_\pm$; together, these provide a complete description of the limit distribution.

These results resolve a long-standing challenge in the study of QWs: the explicit generalization of the Konno distribution to higher dimensions, a task that had remained elusive for general models.

Methodologically, our success depends on completely resolving the noninjective velocity map. By partitioning the wave-vector space based on the zeros of the Jacobian, which define the caustics, we overcame the complexities of singular asymptotics inherent to 2D models.

Our approach provides a foundation for exploring extensions to other 2D models, such as QWs on different lattice structures or those with multistate coins. Regarding higher-dimensional extensions, the redundant cosine representation and the nonlocality of the arccos function make the analytical inversion of the velocity map algebraically intractable. However, this complexity suggests that higher-dimensional DTQWs could exhibit a diverse range of limiting distributions beyond simple 1D combinations. While predicting exact forms for $d \geqslant 3$ remains an open challenge, our 2D analysis provides a glimpse into the potential beauty of these higher-dimensional QWs.

Finally, the relationship between the asymptotic behavior of our discrete (space-time) QW model and the dynamics of a continuum analog, such as the massive Dirac equation in $(2 + 1)$ dimensions, remains an intriguing direction. Our 2D Konno functions $(v_{\max} < 1)$ may serve as a signature of the mass term, contrasting with the massless dynamics of the $v_{\max} = 1$ regime.

ACKNOWLEDGMENTS

We thank C. Cedzich for his helpful remarks and for bringing Refs. [81,85] to our attention. This work was supported by the Japan Society for the Promotion of Science (JSPS) KAKENHI Grants No. JP23K03229 and No. JP24K06851 and by the Research Institute for Mathematical Sciences, an International Joint Usage/Research Center located at Kyoto University.

DATA AVAILABILITY

No data were created or analyzed in this study.

APPENDIX A: PROOFS OF LEMMAS

1. Proof of Lemma 1

The relations $e^{-i\boldsymbol{\theta}\cdot\boldsymbol{x}} S_j e^{i\boldsymbol{\theta}\cdot\boldsymbol{x}} = e^{i\theta_j\sigma_z} S_j = S_j e^{i\theta_j\sigma_z}$, and $C'_j = e^{i\delta_j/2} e^{i\psi_j\sigma_z} C_j e^{i\varphi_j\sigma_z}$ with $\psi_j = (\alpha_j + \beta_j)/2$ and $\varphi_j = (\alpha_j - \beta_j)/2$ prove

$$e^{-i(\delta_1+\delta_2)/2} U' = (e^{-i\varphi_1\sigma_z} e^{i\boldsymbol{\theta}\cdot\boldsymbol{x}}) U (e^{-i\boldsymbol{\theta}\cdot\boldsymbol{x}} e^{i\varphi_1\sigma_z}),$$

with $\boldsymbol{\theta} = (\varphi_1 + \psi_2, \psi_1 + \varphi_2)$. Taking $\gamma = (\delta_1 + \delta_2)/2$ and $W = e^{-i\varphi_1\sigma_z} e^{i\theta\cdot x}$, we obtain (i).

Using the spectral decomposition $\hat{\boldsymbol{x}} = \sum_{\boldsymbol{x}\in\mathbb{Z}^2} \boldsymbol{x}\hat{\Pi}_{\boldsymbol{x}}$ of the position operator, one observes that $\Psi_t^\dagger(\boldsymbol{x})\Psi_t(\boldsymbol{x}) = \langle\Psi_t, \hat{\Pi}_{\boldsymbol{x}}\Psi_t\rangle_{\mathcal{H}}$. Combining this with (i) yields (ii) because W commutes with $\hat{\Pi}_{\boldsymbol{x}}$, i.e., $[W, \hat{\Pi}_{\boldsymbol{x}}] = 0$.

2. Proof of Lemma 2

We only prove that Φ_{12} is a one-to-one onto correspondence. Because $(a, b) \in \Delta$ satisfies $0 \leqslant a + b \leqslant 1, -1 \leqslant a - b \leqslant 1$, and $|a - b| \leqslant a + b$, one can define

$$e^{-i(\delta_1+\delta_2)/2}U' = (e^{-i\varphi_1\sigma_z}e^{i\boldsymbol{\theta}\cdot\boldsymbol{x}})U(e^{-i\boldsymbol{\theta}\cdot\boldsymbol{x}}e^{i\varphi_1\sigma_z}),$$

$$\theta_1 = \tfrac{1}{2}[\arccos(a-b) + \arccos(a+b)], \tag{A1}$$

$$\theta_2 = \tfrac{1}{2}[\arccos(a-b) - \arccos(a+b)], \tag{A2}$$

so that $\theta_j \in [0, \pi/2]$ $(j = 1, 2)$. Then $a_j := \cos\theta_j$ and $b_j := \sin\theta_j$ satisfy $a = a_1a_2$, $b = b_1b_2$, and $(a_1, a_2) \in A_{12}$. Thus Φ_{12} is an onto map.

Suppose that there exists another pair $(a_1', a_2') \in A_{12}$ so that $a = a_1'a_2'$. Then $\theta_j' = \arccos a_j' \in [0, \pi/2]$ $(j = 1, 2)$ satisfy $b_j' = \sin\theta_j'$ $(j = 1, 2)$ and $a \pm b = \cos(\theta_1' \mp \theta_2')$. Substituting these equations into the RHS of (A1) and (A2) yields $\theta_j' = \theta_j$ $(j = 1, 2)$. Thus Φ_{12} is a one-to-one map. Therefore, we obtain the lemma.

3. Proof of Lemma 3

By assumption, $v_{\max} = a + b < 1$. (1) follows by definition. By the arithmetic and geometric mean relation,

$$\begin{aligned} F_0 - \sqrt{F_1F_2} &\geqslant F_0 - (F_1 + F_2)/2 \\ &\geqslant [1 - (a+b)][1 - (a-b)^2]/(2ab) \end{aligned}$$

holds in $E_1 \cap E_2$. (2) follows since the LHS of the above inequality is strictly positive by assumption. The facts that $E_1 \cap E_2 \subset \sigma(\hat{v}_1) \times \sigma(\hat{v}_2)$ and hence that

$$\left(1 - v_1^2\right)\left(1 - v_2^2\right) > (1 - v_{\max}^2)^2$$

in $E_1 \cap E_2$ proves (3).

APPENDIX B: PROOF OF PROPOSITION 2

Let $g = \tilde{h}\tilde{K}_\pm$ and $I_j = \iint_{\tilde{D}_j} g\, dv du$ for $j = 1, 2$.

We first prove $\lim_{b\to 0} I_1 = 0$. Lemma 3 states that $K_\pm \leqslant F_0/\sqrt{F_1F_2}$ and $abF_0 \leqslant 1$ on $E_1 \cap E_2$. Using the identity $(a_jb_j)^2\tilde{F}_j = a_j^2(r_j^2 - u^2)$ $(j = 1, 2)$ obtained by definition yields

$$g \lesssim \frac{1}{ab\sqrt{\tilde{F}_1\tilde{F}_2}} = \frac{1}{a\sqrt{\left(r_1^2 - u^2\right)\left(r_2^2 - u^2\right)}}$$

on $\tilde{D}_1 \cup \tilde{D}_2$, where $g_1 \lesssim g_2$ for functions g_1 and g_2 indicates that g_1/g_2 is bounded above by a constant independent of the variables of g_1 and g_2. Observe that

$$r_2^2 - u^2 \geqslant r_2^2 - r_1^2 = \frac{b_1^2 - b_2^2}{a^2}(v^2 - a^2) > 0 \text{ on } \tilde{D}_1.$$

Combining these inequalities and using the symmetry of $\tilde{D}_j$ and the integrand yields

$$I_1 \lesssim \int_a^{a_1} \frac{dv}{\sqrt{v^2 - a^2}} \int_0^{r_1} \frac{du}{\sqrt{r_1^2 - u^2}} = \frac{\pi}{2}\ln\left(1 + \frac{b_2}{a_2}\right),$$

where the RHS tends to zero as $b_2 \to 0$. The last equality follows from the following formulas (up to constants)

$$\int \frac{dx}{\sqrt{|x^2 - s^2|}} = \begin{cases} \arcsin\dfrac{x}{s}, & s > |x| \\ \log(x + \sqrt{x^2 - s^2}), & |x| > |s|. \end{cases}$$

We next examine the limit of I_2 as $b \to 0$. Observe that r_2 tends to zero as $b_2 \to 0$ and that $b_2^2\tilde{F}_2(v, r_2u_2) = r_2^2(1 - u_2^2)$. The change of variables $u_2 = u/r_2$ yields

$$\begin{aligned} I_2 &= r_2 \int_{-a}^{a} dv \int_{-1}^{1} du_2 \tilde{h}(v, r_2u_2)\tilde{K}_\pm(v, r_2u_2) \\ &\sim \frac{b_1}{4} \int_{-a_1}^{a_1} dv \frac{(1 - v^2)\tilde{h}(v, 0)}{\sqrt{a_1^2 - v^2}} \int_{-1}^{1} \frac{du_2}{\sqrt{1 - u_2^2}} \end{aligned}$$

as $b \to 0$, where $A \sim B$ for constants A and B depending on b denotes $|A - B| = o(b)$ as $b \to 0$. The desired result then follows from the Lebesgue convergence theorem and calculating the integral directly.

APPENDIX C: PROOF OF PROPOSITION 6

In this proof, the quadratic form $\varphi(\boldsymbol{c})$ defined in (31) plays a key role. We now define a single-variable quadratic polynomial $\varphi_1(x)$ by $\varphi_1(x) = \varphi(1, x)$. The discriminant $D_1 = [1 - (a - b)^2][1 - (a + b)^2]$ of $\varphi_1(x)$ is always non-negative if $a + b \leqslant 1$; D_1 attains zero only when $a + b = 1$. Thus, φ_1 has two zeros if $a + b < 1$ and one zero if $a + b = 1$; Writing the zeros as $j_\pm$ with ordering $j_+ \geqslant j_-$ observes that the lines $c_2 = j_\pm c_1$ partition the square $[-1, 1]^2$ in the c_1c_2 plane into four regions (as depicted in Fig. 8) $C^{(m)}$ $(m = 1, 2, 3, 4)$ if $a + b < 1$, and into two regions $C^{(2)}, C^{(4)}$ if $a + b = 1$. The factorization $\varphi_1(x) = ab(x - j_+)(x - j_-)$ and the identity $\varphi(\boldsymbol{c}) = c_1^2\varphi_1(c_2/c_1)$ yield the identity

$$\varphi(\boldsymbol{c}) = ab(c_2 - j_+c_1)(c_2 - j_-c_1),$$

which determines the sign of the quadratic form $\varphi(\boldsymbol{c})$ and proves that $\varphi(\boldsymbol{c}) = 0$ holds only on the lines $c_2 = j_\pm c_1$; otherwise $\operatorname{sgn}\varphi(\boldsymbol{c}) = (-1)^m$ on $C^{(m)}$. Combining this with the relation (30) ensures that $J = 0$ on the lines $c_2 = j_\pm c_1$, otherwise $|J|^{-1} = |J|^{-1}_{(-1)^m}$

APPENDIX D: PROOF OF THEOREM 6

In this Appendix, we determine the joint spectrum $\Sigma(\hat{\boldsymbol{v}})$, which is the closure of the image of the velocity map $\boldsymbol{v}(\boldsymbol{k})$. We focus on the $(a, b) \in \Delta_{(0,1)}$ case (where $v_{\max} < 1$); the Δ_1 case (where $v_{\max} = 1$) is addressed at the end.

The proof becomes clear with the change of variables $\boldsymbol{u} = (v_1 + v_2, v_1 - v_2)/\sqrt{2}$, which corresponds to a standard rotation of the coordinate system by $\pi/4$. Equation (27) then provides

$$u_1 = -\frac{\sqrt{2}as_1}{\sqrt{1 - \tau^2}}, \quad u_2 = -\frac{\sqrt{2}bs_2}{\sqrt{1 - \tau^2}}. \tag{D1}$$

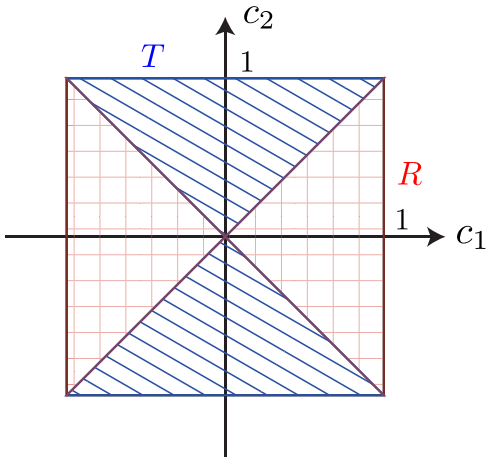


FIG. 9. Division of $[-1,1]^2$ into R and T in c_1c_2 plane. The region shaded with red grids in the shape of a ribbon represents R, while the region shaded with blue diagonal lines in the shape of a twister represents T.

Here, $\boldsymbol{u}$ depends on $\boldsymbol{c}=(c_1,c_2)$ and the signs of s_i. Since the signs of s_i (and thus the signs of u_1,u_2) are uniquely determined by the index n via Table IV, the map $\boldsymbol{u}$ exhibits symmetry across the quadrants. To analyze the image, we follow the partitioning scheme introduced in Sec. V C 2. We first partition the $[-1,1]^2$ in the c_1c_2 plane into the regions R and T (see Fig. 9):

$$R := \{\boldsymbol{c}=(c_1,\kappa c_1) \mid c_1\in[-1,1],\kappa\in[-1,1]\},$$
$$T := \{\boldsymbol{c}=(\gamma c_2,c_2) \mid c_2\in[-1,1],\gamma\in[-1,1]\}.$$

The domains $K_{n,s}$ (for $s=R,T$) are then defined as the pullbacks of these regions into the nth windmill domain K_n. The labels $\boldsymbol{u}(R)$ and $\boldsymbol{u}(T)$ in Fig. 10 correspond to the union of the images:

$$\boldsymbol{u}(R)=\bigcup_{n=1}^{4}\boldsymbol{u}(K_{n,R}),\quad \boldsymbol{u}(T)=\bigcup_{n=1}^{4}\boldsymbol{u}(K_{n,T}).$$

We now show that the union of the images $\boldsymbol{u}(R)$ and $\boldsymbol{u}(T)$ corresponds to the $\pi/4$ rotation of $E_1\cap E_2$, as illustrated in Fig. 10. To analyze the image $\boldsymbol{u}(R)$, we square two equations in (D1) and substitute $c_2=\kappa c_1$ into them. Eliminating c_1^2 from these equations yields

$$\frac{u_1^2}{-f_{R,1}(\kappa)}+\frac{u_2^2}{f_{R,2}(\kappa)}=1, \tag{D2}$$

where $f_{R,1}$ and $f_{R,2}$ are functions of the parameter κ. The explicit definitions of these functions and their analysis are provided in Fig. 11. As shown there, (D2) describes ellipses (when $f_{R,1}<0$) or hyperbolas (when $f_{R,1}>0$). As κ varies, the union of these curves fills the regions $\boldsymbol{u}(R)$. The values $\kappa=\pm1$ define the boundaries between $\boldsymbol{u}(R)$ and $\boldsymbol{u}(T)$, while $\kappa=j_+$ (given Sec. V C 2) provides the maximal extent of the full image.

These functions $f_{R,1}$ and $f_{R,2}$, at this critical point, take $f_{R,1}(j_+)=-2(a_1\vee a_2)^2$ and $f_{R,2}(j_+)=2(b_1\wedge b_2)^2$, and

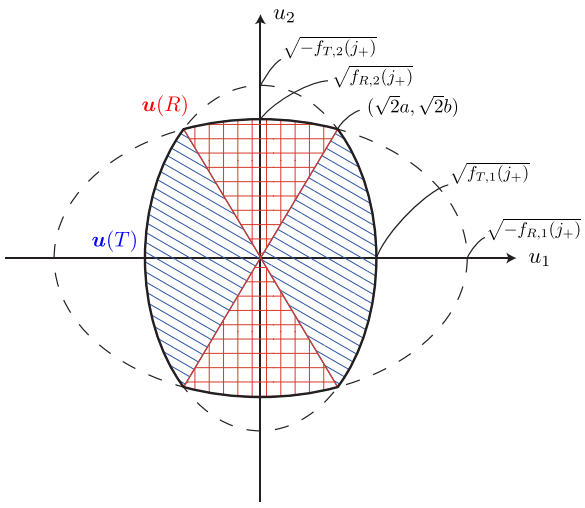


FIG. 10. The joint spectrum $\Sigma(\hat{\boldsymbol{v}})$ visualized in the $\pi/4$-rotated coordinate system $\boldsymbol{u}=(u_1,u_2)$. The full domain (shaded) is the intersection of two ellipses, corresponding to $E_1\cap E_2$ in Fig. 3. It is partitioned into the image $\boldsymbol{u}(R)$ (red grids) and $\boldsymbol{u}(T)$ (blue diagonal lines), which originate from the R and T regions defined in Fig. 9. The dashed curves show the boundaries of the two individual ellipses (E_1 and E_2). These boundaries are generated by the critical values $\kappa=j_+$ or $\gamma=j_+$, where $\kappa\in[-1,1]$ is a parameter of (D2) and so is γ, and their maximal extents are marked by the labeled axis intercepts [e.g., $\sqrt{f_{T,1}(j_+)}$ and $\sqrt{f_{R,2}(j_+)}$].

hence (D2) forms the boundary ellipse:

$$\frac{u_1^2}{2(a_1\vee a_2)^2}+\frac{u_2^2}{2(b_1\wedge b_2)^2}=1, \tag{D3}$$

where $x\wedge y:=\min\{x,y\}$ and $x\vee y:=\max\{x,y\}$. By similar calculations for T, the boundary $\gamma=j_+$ (i.e., $c_2=j_-c_1$) yields the other ellipse:

$$\frac{u_1^2}{2(a_1\wedge a_2)^2}+\frac{u_2^2}{2(b_1\vee b_2)^2}=1. \tag{D4}$$

Since $\boldsymbol{u}(R)\cup\boldsymbol{u}(T)$ is the intersection of two ellipses bounded by (D3) and (D4), it is precisely the $\pi/4$-rotated image of $E_1\cap E_2$, which proves $\Sigma(\hat{\boldsymbol{v}})=E_1\cap E_2$.

When $(a,b)\in\Delta_1$, the parameters degenerate as $j_\pm=-1$. This is a crucial difference from the $(a,b)\in\Delta_{(0,1)}$ case: the caustic boundary (i.e., $\kappa=j_+$) now merges with the R/T partition boundary $\kappa=-1$. In this degenerate case, the caustic boundary no longer maps to a curve, but collapses to the four discrete points $\pm(\sqrt{2}a,\sqrt{2}b)$ and $\pm(\sqrt{2}a,-\sqrt{2}b)$, which are located at the boundary $u_1^2/(2a)+u_2^2/(2b)=1$ of the $\pi/4$-rotated image of the ellipse E. The other boundary $\kappa=1$ and the entire interior of $[-1,1]^2$ in the c_1c_2 plane both map to the open interior of the above ellipse. Therefore, the image of the map $\boldsymbol{u}=\boldsymbol{u}(\boldsymbol{c})$ is the open single elliptical region plus four discrete boundary points. As the joint spectrum must be closed, we observe $\Sigma(\hat{\boldsymbol{v}})=E$.

APPENDIX E: DERIVATION OF 1D LIMITS

Here we sketch the proofs of Theorems 2 and 4. The proofs are based on the fact that the 2D velocity operators $\hat{v}_1$ and $\hat{v}_2$

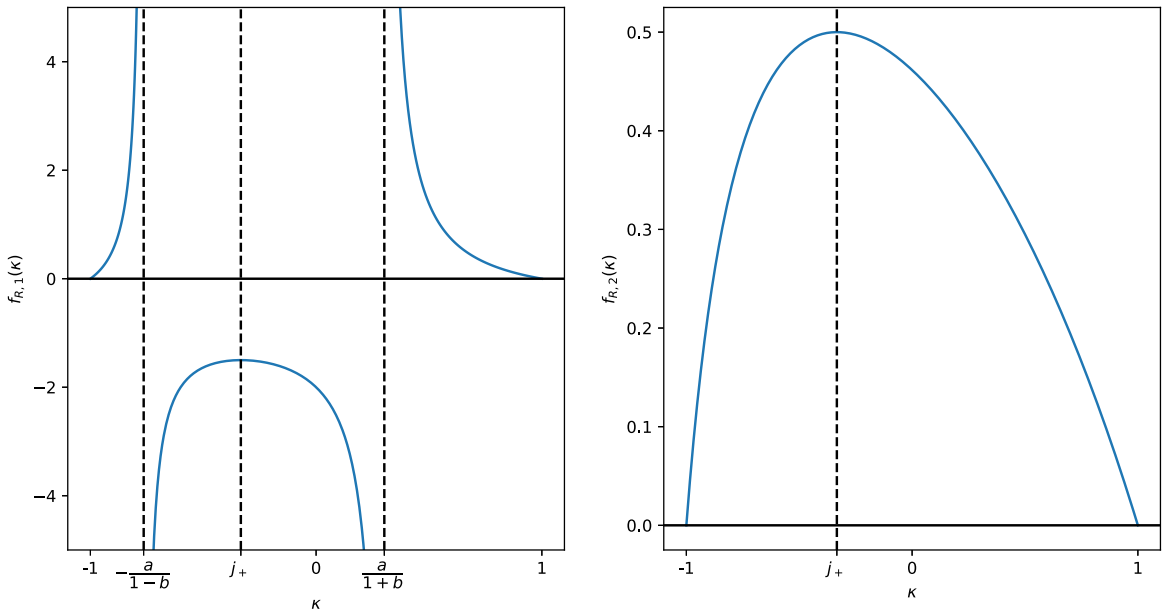


FIG. 11. Graphs of the functions $f_{R,1}(\kappa)$ (left) and $f_{R,2}(\kappa)$ (right), defined as $f_{R,1}(\kappa) = [2a^2(1-\kappa^2)]/[\kappa^2 - (a-b\kappa)^2]$, $f_{R,2}(\kappa) = [2b^2(1-\kappa^2)]/[1-(a-b\kappa)^2]$ for $\kappa \in [-1, 1]$. These functions determine the geometry of the image $\boldsymbol{u}(R)$ via (D2). The plot of $f_{R,1}$ illustrates its alternating sign, diverging at the vertical asymptotes $\kappa = -a/(1-b)$ and $\kappa = a/(1+b)$. In contrast, $f_{R,2}(\kappa)$ is strictly positive for $\kappa \in (-1, 1)$. Both functions have a maximal at $\kappa = j_+$—specifically, a maximum for $f_{R,2}(\kappa)$ and a local maximum for $f_{R,1}(\kappa)$—which corresponds to the maximal extent of the image $\boldsymbol{u}(R)$.

both converge to the direct sum of copies of the 1D velocity operator $\hat{v}_{\mathrm{K}}$ in the 1D limit $b \to 0$.

Recall that the 1D velocity operator $\hat{v}_{\mathrm{K}}(k)$ for a translation invariant 1D2SQW with the evolution

$$\hat{U}_{\mathrm{K}}(k) = \begin{pmatrix} e^{ik} & 0 \\ 0 & e^{-ik} \end{pmatrix} \begin{pmatrix} a_1 & b_1 \\ -b_1 & a_1 \end{pmatrix}$$

in the wave number space $\mathbb{T}$ is defined as follows [37,63]. Let $e^{\pm i\omega_{\mathrm{K}}(k)}$ be the eigenvalue of $\hat{U}_{\mathrm{K}}(k)$, where the dispersion relation is $\omega_{\mathrm{K}}(k) = \arccos(a_1 \cos k)$. The 1D group velocity is then given by

$$v_{\mathrm{K}}(k) := -\frac{a_1 \sin k}{\sqrt{1-(a_1 \cos k)^2}}, \tag{E1}$$

which is consistent with the sign convention of the group velocity as defined in Sec. V A. The 1D velocity operator $\hat{v}_{\mathrm{K}}(k)$ is defined as

$$\hat{v}_{\mathrm{K}}(k) = \sum_{\star=\pm} v_{\mathrm{K},\star}(k) |\omega_{\mathrm{K},\star}(k)\rangle\langle\omega_{\mathrm{K},\star}(k)|, \tag{E2}$$

where $v_{\mathrm{K},\pm}(k) := \pm v_{\mathrm{K}}(k)$, and the corresponding eigenvectors are

$$|\omega_{\mathrm{K},\pm}(k)\rangle = \frac{1}{\sqrt{2}} \begin{pmatrix} e^{ik}\sqrt{1 \mp v_{\mathrm{K}}(k)} \\ \pm i\sqrt{1 \pm v_{\mathrm{K}}(k)} \end{pmatrix}, \tag{E3}$$

which form an ONB of $\mathbb{C}^2$.

As explained immediately after Definition 1, the 2D evolution $U_{(a,b)}$ converges in the 1D limit to the 1D evolution U_{a_1}, which is identical to the operator in the $\Delta_{ab=0}$ regime (see Table II). As mentioned in Sec. III B, such an operator can decouple into an infinite direct sum of 1D motions, each governed by the evolution $\tilde{S}_{1\mathrm{D}}C_1$. Identifying $\ell^2(\mathbb{L}_n^{(+)}; \mathbb{C}^2)$ with $\ell^2(\mathbb{Z}; \mathbb{C}^2)$ shows that $\tilde{S}_{1\mathrm{D}}C_1$ is unitarily equivalent to U_{K}, i.e., the position representation of $\hat{U}_{\mathrm{K}}$ stated above. Implementing this identification by $\hat{\psi}_0^{(n)}(m) := \Psi_0(m, n+m)$ provides

$$\hat{\Psi}_0(\boldsymbol{k}) = \sum_{n\in\mathbb{Z}} e^{-ink_2} \hat{\psi}_0^{(n)}(k_1 + k_2), \tag{E4}$$

where $\Psi_0 \in \mathcal{H}$ is the initial state and $\hat{\psi}_0^{(n)}$ denotes the 1D Fourier transform of $\psi_0^{(n)}$.

The remainder of this appendix uses the terminology defined in Eqs. (24)–(28) and (29). To emphasize the dependence on b, we denote the 2D velocity operators by $\hat{\boldsymbol{v}}_b = (\hat{v}_{1,b}, \hat{v}_{2,b})$. Similarly, we use $\boldsymbol{v}_b(\boldsymbol{k}) = (v_{1,b}(\boldsymbol{k}), v_{2,b}(\boldsymbol{k}))$ to denote the 2D velocity map.

1. 1D limits for velocity operators

In this appendix, we show that the 1D limit $b \to 0$ decouples the 2D velocity operators $\hat{v}_j$ into an infinite direct sum of copies of the 1D velocity operator $\hat{v}_{\mathrm{K}}$. Specifically, we prove the following: Let

$$P_{\mathrm{K},\star}^{(n)}(k) = \left|\langle\omega_{\mathrm{K},\star}(k)|\hat{\psi}_0^{(n)}(k)\rangle\right|^2. \tag{E5}$$

Proposition E 1. For any continuous function g,

$$\lim_{b\to 0} \int_{\Sigma(\hat{\boldsymbol{v}}_b)} g(\boldsymbol{v})\, d\langle\Psi_0|E_{\hat{\boldsymbol{v}}_b}(\boldsymbol{v})\Psi_0\rangle = \sum_{n\in\mathbb{Z}} \sum_{\star=\pm} \int_{-\pi}^{\pi} \frac{dk}{2\pi} g(v_{\mathrm{K},\star}(k), v_{\mathrm{K},\star}(k)) P_{\mathrm{K},\star}^{(n)}(k). \tag{E6}$$

Proof. By definitions, the 1D limit $b \to 0$ (which implies $b = 0$ and $a = a_1$) of the 2D velocity map $\boldsymbol{v}_b$ is a one-variable function of $l_1 = k_1 + k_2$: $\lim_{b\to 0} v_{j,b}(\boldsymbol{k}) = v_{\mathrm{K}}(l_1)$ with v_{K} de-

fined in (E1). The eigenvectors of $\hat{v}_{j,b}$ are represented as

$$|\omega_\pm(\boldsymbol{k})\rangle = \frac{1}{\sqrt{2}}\begin{pmatrix} e^{i\eta_b(\boldsymbol{k})}\sqrt{1 \mp v_{2,b}(\boldsymbol{k})} \\ \pm i\sqrt{1 \pm v_{2,b}(\boldsymbol{k})} \end{pmatrix},$$

with the argument $\eta_b(\boldsymbol{k})$ of $a_2 b_1 e^{il_1} + b_2 a_1 e^{il_2}$. By $\lim_{b\to 0} e^{i\eta_b(\boldsymbol{k})} = e^{il_1}$, we obtain $\lim_{b\to 0} |\omega_\star(\boldsymbol{k})\rangle = |\omega_{\mathrm{K},\star}(l_1)\rangle$, which are also functions of l_1. Applying these limits to the decomposition (23) shows the pointwise convergence $\lim_{b\to 0} \hat{v}_{j,b}(\boldsymbol{k}) = \hat{v}_{\mathrm{K}}(l_1)$, where $\hat{v}_{\mathrm{K}}$ is the 1D velocity operator defined in (E2). Using the spectral decomposition and (E4), we observe that

$$\begin{aligned} &\text{LHS of (E6)} \\ &= \sum_{\star=\pm}\sum_{n,n'} \int_{\mathbb{T}^2} \frac{d\boldsymbol{k}}{(2\pi)^2} g(v_{\mathrm{K},\star}(l_1), v_{\mathrm{K},\star}(l_1)) e^{i(n'-n)k_2} \\ &\quad \times \langle \hat{\psi}_0^{(n')}(l_1)|\omega_{\mathrm{K},\star}(l_1)\rangle\langle\omega_{\mathrm{K},\star}(l_1)|\hat{\psi}_0^{(n)}(l_1)\rangle. \end{aligned}$$

After changing variables to $(k, k') = (k_1 + k_2, k_2)$, periodicity ensures that k' only appears in the factor $e^{i(n-n')k'}/(2\pi)$. Integrating this factor simplifies the sum over n' and yields (E6).■

2. 1D limit in $\Delta_{(a,b)}$ regime

We prove Theorem 2. By the definition of $\rho_{(a,b)}$ and Proposition 7, we need only calculate the RHS of (E6). Following Ref. [66], Lemma 4.6], we define the 1D inverse velocity map $k = k_{\star,m}(v)$, which appeared in (4), as follows. We divide $\mathbb{T}$ into $\mathbb{T}_0 = [-\pi/2, \pi/2]$ and $\mathbb{T}_1 = [\pi/2, 3\pi/2]$, where the restrictions $v_{\mathrm{K},\star}|_{\mathbb{T}_m}$ ($\star = \pm$, $m = 0, 1$) of the velocity map $v = v_{\mathrm{K},\star}$ are invertible. The resulting inverse functions are given by

$$k_{\pm,m}(v) = m\pi + \arcsin\left(\frac{\mp(-1)^m b_1 v}{a_1\sqrt{1-v^2}}\right) \tag{E7}$$

for $v \in [-a_1, a_1]$, whose derivatives, as mentioned at the end of Sec. I A, provide the Konno function f_{K}.

Changing variables by $k = k_{\pm,m}(v)$ allows us to represent

$$\lim_{b_2\to 0}\int_{\Sigma(\hat{\boldsymbol{v}})} g(\boldsymbol{v})\rho_{(a,b)}(\boldsymbol{v})d\boldsymbol{v} = \int_{-a_1}^{a_1} g(v,v)\rho_{a_1}(v)dv,$$

where $\rho_{a_1}(v) = w(v; a_1) f_{\mathrm{K}}(v; a_1)$ given in (19) is the 1D limit of $\rho_{(a,b)}(v)$ and the weight $w(v; a_1)$ is given by

$$w(v; a_1) = \frac{1}{2}\sum_{\substack{n\in\mathbb{Z} \\ \star=\pm,\ m=0,1}} P^{(n)}_{\mathrm{K},\star}(k_{\star,m}(v)), \tag{E8}$$

where $P^{(n)}_{\mathrm{K},\star}(k)$ and $k_{\star,m}(v)$ are defined in (E5) and (E7).

3. 1D limit in Δ_1 regime

We prove Theorem 4. The 1D limit in the Δ_1 regime corresponds to the 1D QW model with $a_1 = 1$. We therefore evaluate the RHS of (E6) for this specific case. Setting $a_1 = 1$ in (E1) simplifies the velocity to $v_{\mathrm{K}}(k) = -\mathrm{sgn}(\sin k)$. Combining this with (E3) allows us to take (up to phase factors) $|\omega_{\mathrm{K},\pm}\rangle$ as

$$\begin{aligned} |\omega_{\mathrm{K},\pm}(k)\rangle &= |\mp\rangle \quad \text{if } v_{\mathrm{K}}(k) = 1, \\ |\omega_{\mathrm{K},\pm}(k)\rangle &= |\pm\rangle \quad \text{if } v_{\mathrm{K}}(k) = -1, \end{aligned}$$

where we define $|\pm\rangle$ so that $\langle\pm|\Psi(x)\rangle = \Psi^{(\pm)}(x)$. Substituting this into (E5) and calculating the RHS of (E6), we use the fact that $v_{\mathrm{K}}(k)$ only takes the discrete values ± 1. The function $g(v_{\mathrm{K},\star}(k), v_{\mathrm{K},\star}(k))$ thus becomes independent of the integration variable k and is factored out, leaving only the integral of $P^{(n)}_{\mathrm{K},\star}(k)$. This yields

$$\begin{aligned} \lim_{b_2\to 0}\int_{\Sigma(\hat{\boldsymbol{v}})} g(\boldsymbol{v})\rho^{(1)}_{(a,b)}(\boldsymbol{v})d\boldsymbol{v} &= \sum_{v=\pm 1} g(v,v)C_v \\ &= \int_{-1}^{1} g(v,v)\rho_1(v)dv, \end{aligned}$$

where $\rho_1(v)$ is defined in (20) and the constants are $C_{\pm 1} = \|\Psi_0^{(\mp)}\|^2_{\ell^2(\mathbb{Z}^2)}$.

[1] M. Kac, Random walk and the theory of Brownian motion, Am. Math. Mon. **54**, 369 (1947).

[2] W. Feller, *An Introduction to Probability Theory and Its Applications* (Wiley, New York, 1968), Vol. 1.

[3] G. H. Weiss, *Aspects and Applications of the Random Walk*, International Congress Series (North-Holland, New York, 1994).

[4] R. Motwani and P. Raghavan, *Randomized Algorithms*, Cambridge International Series on Parallel Computation (Cambridge University Press, Cambridge, 1995).

[5] G. Grimmett and D. Stirzaker, *Probability and Random Processes*, 4th ed., Oxford Science Publications (Oxford University Press, Oxford, 2020).

[6] L. Yang, Z. Zhang, Y. Song, S. Hong, R. Xu, Y. Zhao, W. Zhang, B. Cui, and M.-H. Yang, Diffusion models: A comprehensive survey of methods and applications, ACM Comput. Surv. **56**, 1 (2023).

[7] R. P. Feynman, Simulating physics with computers, Int. J. Theor. Phys. **21**, 467 (1982).

[8] P. Benioff, The computer as a physical system: A microscopic quantum mechanical Hamiltonian model of computers as represented by Turing machines, J. Stat. Phys. **22**, 563 (1980).

[9] D. Deutsch and R. Jozsa, Rapid solution of problems by quantum computation, Proc. A **439**, 553 (1992).

[10] L. K. Grover, A fast quantum mechanical algorithm for database search, in *Proceedings of the Twenty-Eighth Annual ACM Symposium on Theory of Computing*, STOC '96 (Association for Computing Machinery, New York, 1996), pp. 212–219.

[11] S. Lloyd, Universal quantum simulators, Science **273**, 1073 (1996).

[12] P. W. Shor, Polynomial-time algorithms for prime factorization and discrete logarithms on a quantum computer, SIAM J. Comput. **26**, 1484 (1997).

[13] D. Horn and A. Gottlieb, Algorithm for data clustering in pattern recognition problems based on quantum mechanics, Phys. Rev. Lett. **88**, 018702 (2001).

[14] A. Aspuru-Guzik, A. D. Dutoi, P. J. Love, and M. Head-Gordon, Simulated quantum computation of molecular energies, Science **309**, 1704 (2005).

[15] A. Perdomo, C. Truncik, I. Tubert-Brohman, G. Rose, and A. Aspuru-Guzik, Construction of model Hamiltonians for adiabatic quantum computation and its application to finding low-energy conformations of lattice protein models, Phys. Rev. A **78**, 012320 (2008).

[16] I. Kassal and A. Aspuru-Guzik, Quantum algorithm for molecular properties and geometry optimization, J. Chem. Phys. **131**, 224102 (2009).

[17] Y. Aharonov, L. Davidovich, and N. Zagury, Quantum random walks, Phys. Rev. A **48**, 1687 (1993).

[18] E. Farhi and S. Gutmann, Quantum computation and decision trees, Phys. Rev. A **58**, 915 (1998).

[19] A. Nayak and A. Vishwanath, Quantum walk on the line, Tech. Rep., Center for Discrete Mathematics & Theoretical Computer Science, 2000.

[20] A. Ambainis, E. Bach, A. Nayak, A. Vishwanath, and J. Watrous, One-dimensional quantum walks, in *Proceedings of the Thirty-Third Annual ACM Symposium on Theory of Computing*, STOC '01 (Association for Computing Machinery, New York, 2001), pp. 37–49.

[21] A. M. Childs, Universal computation by quantum walk, Phys. Rev. Lett. **102**, 180501 (2009).

[22] N. B. Lovett, S. Cooper, M. Everitt, M. Trevers, and V. Kendon, Universal quantum computation using the discrete-time quantum walk, Phys. Rev. A **81**, 042330 (2010).

[23] A. M. Childs, D. Gosset, and Z. Webb, Universal computation by multiparticle quantum walk, Science **339**, 791 (2013).

[24] A. Ambainis, Quantum walks and their algorithmic applications, Int. J. Quantum Inform. **01**, 507 (2003).

[25] A. M. Childs, R. Cleve, E. Deotto, E. Farhi, S. Gutmann, and D. A. Spielman, Exponential algorithmic speedup by a quantum walk, in *Proceedings of the Thirty-Fifth Annual ACM Symposium on Theory of Computing*, STOC '03 (Association for Computing Machinery, New York, 2003), pp. 59–68.

[26] M. Szegedy, Quantum speed-up of Markov chain based algorithms, in *Proceedings of the 45th Annual IEEE Symposium on Foundations of Computer Science*, FOCS '04 (IEEE Computer Society, USA, 2004), pp. 32–41.

[27] G. Varsamis, I. Karafyllidis, K. Gilkes, U. Arranz, R. Martin-Cuevas, G. Calleja, J. Wong, H. Jessen, P. Dimitrakis, P. Kolovos, and R. Sandaltzopoulos, Quantum algorithm for *de novo* DNA sequence assembly based on quantum walks on graphs, BioSystems **233**, 105037 (2023).

[28] I. Bialynicki-Birula, Weyl, Dirac, and Maxwell equations on a lattice as unitary cellular automata, Phys. Rev. D **49**, 6920 (1994).

[29] D. A. Meyer, From quantum cellular automata to quantum lattice gases, J. Stat. Phys. **85**, 551 (1996).

[30] S. Succi and R. Benzi, Lattice Boltzmann equation for quantum mechanics, Phys. D: Nonlinear Phenom. **69**, 327 (1993).

[31] B. M. Boghosian and W. Taylor, IV, Simulating quantum mechanics on a quantum computer, Phys. D: Nonlinear Phenom. **120**, 30 (1998).

[32] M. Mohseni, P. Rebentrost, S. Lloyd, and A. Aspuru-Guzik, Environment-assisted quantum walks in photosynthetic energy transfer, J. Chem. Phys. **129**, 174106 (2008).

[33] T. Kitagawa, M. A. Broome, A. Fedrizzi, M. S. Rudner, E. Berg, I. Kassal, A. Aspuru-Guzik, E. Demler, and A. G. White, Observation of topologically protected bound states in photonic quantum walks, Nat. Commun. **3**, 882 (2012).

[34] S. Panahiyan and S. Fritzsche, Simulation of the multiphase configuration and phase transitions with quantum walks utilizing a step-dependent coin, Phys. Rev. A **100**, 062115 (2019).

[35] N. Konno, Quantum random walks in one dimension, Quantum Inf. Process. **1**, 345 (2002).

[36] N. Konno, A new type of limit theorems for the one-dimensional quantum random walk, J. Math. Soc. Jpn. **57**, 1179 (2005).

[37] G. Grimmett, S. Janson, and P. F. Scudo, Weak limits for quantum random walks, Phys. Rev. E **69**, 026119 (2004).

[38] N. Inui, N. Konno, and E. Segawa, One-dimensional three-state quantum walk, Phys. Rev. E **72**, 056112 (2005).

[39] N. Konno, Limit theorem for continuous-time quantum walk on the line, Phys. Rev. E **72**, 026113 (2005).

[40] T. Miyazaki, M. Katori, and N. Konno, Wigner formula of rotation matrices and quantum walks, Phys. Rev. A **76**, 012332 (2007).

[41] E. Segawa and N. Konno, Limit theorems for quantum walks driven by many coins, Int. J. Quantum Inform. **06**, 1231 (2008).

[42] N. Konno, Quantum walks, in *Quantum Potential Theory*, edited by P. Biane, L. Bouten, F. Cipriani, N. Konno, N. Privault, Q. Xu, U. Franz, and M. Schürmann (Springer, Berlin, Heidelberg, 2008), pp. 309–452.

[43] C. Liu and N. Petulante, One-dimensional quantum random walks with two entangled coins, Phys. Rev. A **79**, 032312 (2009).

[44] K. Chisaki, M. Hamada, N. Konno, and E. Segawa, Limit theorems for discrete-time quantum walks on trees, Interdiscip. Inf. Sci. **15**, 423 (2009).

[45] N. Konno, One-dimensional discrete-time quantum walks on random environments, Quantum Inf. Process. **8**, 387 (2009).

[46] N. Konno and T. Machida, Limit theorems for quantum walks with memory, Quantum Inf. Comput. **10**, 1004 (2010).

[47] T. Machida and N. Konno, Limit theorem for a time-dependent coined quantum walk on the line, in *Natural Computing: 4th International Workshop on Natural Computing Himeji, Japan, September 2009 Proceedings*, edited by F. Peper, H. Umeo, N. Matsui, and T. Isokawa (Springer Japan, 2010), pp. 226–235.

[48] T. Machida, Limit theorems for a localization model of 2-state quantum walks, Int. J. Quantum Inform. **09**, 863 (2011).

[49] C. Liu, Asymptotic distributions of quantum walks on the line with two entangled coins, Quantum Inf. Process. **11**, 1193 (2012).

[50] K. Chisaki, N. Konno, and E. Segawa, Limit theorems for the discrete-time quantum walk on a graph with joined half lines, Quantum Inf. Comput. **12**, 314 (2012).

[51] A. Wójcik, T. Łuczak, P. Kurzyński, A. Grudka, T. Gdala, and M. Bednarska-Bzdęga, Trapping a particle of a quantum walk on the line, Phys. Rev. A **85**, 012329 (2012).

[52] N. Konno and H. J. Yoo, Limit theorems for open quantum random walks, J. Stat. Phys. **150**, 299 (2013).

[53] C. Liu and N. Petulante, Weak limits for quantum walks on the half-line, Int. J. Quantum Inform. **11**, 1350054 (2013).

[54] N. Konno, T. Łuczak, and E. Segawa, Limit measures of inhomogeneous discrete-time quantum walks in one dimension, Quantum Inf. Process. **12**, 33 (2013).
[55] T. Machida, Realization of the probability laws in the quantum central limit theorems by a quantum walk, Quantum Info. Comput. **13**, 430 (2013).
[56] T. Tate, An algebraic structure for one-dimensional quantum walks and a new proof of the weak limit theorem, Infin. Dimens. Anal. Quantum Probab. Relat. Top. **16**, 1350018 (2013).
[57] Y. Shikano, From discrete time quantum walk to continuous time quantum walk in limit distribution, J. Comp. Theor. Nanosci. **10**, 1558 (2013).
[58] T. Endo and N. Konno, The stationary measure of a space-inhomogeneous quantum walk on the line, Yokohama Math. J. **60**, 33 (2014).
[59] T. Endo, N. Konno, E. Segawa, and M. Takei, A one-dimensional Hadamard walk with one defect, Yokohama Math. J. **60**, 49 (2014).
[60] N. Konno, The uniform measure for discrete-time quantum walks in one dimension, Quantum Inf. Process. **13**, 1103 (2014).
[61] S. Falkner and S. Boettcher, Weak limit of the three-state quantum walk on the line, Phys. Rev. A **90**, 012307 (2014).
[62] N. Konno and M. Takei, The non-uniform stationary measure for discrete-time quantum walks in one dimension, Quantum Inf. Comput. **15**, 1060 (2015).
[63] A. Suzuki, Asymptotic velocity of a position-dependent quantum walk, Quantum Inf. Process. **15**, 103 (2016).
[64] S. Endo, T. Endo, N. Konno, E. Segawa, and M. Takei, Weak limit theorem of a two-phase quantum walk with one defect, Interdiscip. Inf. Sci. **22**, 17 (2016).
[65] S. Richard, A. Suzuki, and R. Tiedra de Aldecoa, Quantum walks with an anisotropic coin I: Spectral theory, Lett. Math. Phys. **108**, 331 (2018).
[66] S. Richard, A. Suzuki, and R. Tiedra de Aldecoa, Quantum walks with an anisotropic coin II: Scattering theory, Lett. Math. Phys. **109**, 61 (2019).
[67] M. Maeda, H. Sasaki, E. Segawa, A. Suzuki, and K. Suzuki, Weak limit theorem for a nonlinear quantum walk, Quantum Inf. Process. **17**, 215 (2018).
[68] T. Fuda, D. Funakawa, and A. Suzuki, Weak limit theorem for a one-dimensional split-step quantum walk, Rev. Roumaine Math. Pures Appl. **64**, 157 (2019).
[69] K. Wada, A weak limit theorem for a class of long-range-type quantum walks in 1d, Quantum Inf. Process. **19**, 2 (2019).
[70] A. Mandal, R. S. Sarkar, S. Chakraborty, and B. Adhikari, Limit theorems and localization of three-state quantum walks on a line defined by generalized Grover coins, Phys. Rev. A **106**, 042405 (2022).
[71] K. Watabe, N. Kobayashi, M. Katori, and N. Konno, Limit distributions of two-dimensional quantum walks, Phys. Rev. A **77**, 062331 (2008).
[72] C. Di Franco, M. Mc Gettrick, T. Machida, and Th. Busch, Alternate two-dimensional quantum walk with a single-qubit coin, Phys. Rev. A **84**, 042337 (2011).
[73] D. A. Meyer, Quantum mechanics of lattice gas automata: One-particle plane waves and potentials, Phys. Rev. E **55**, 5261 (1997).
[74] D. A. Meyer, Quantum mechanics of lattice gas automata: Boundary conditions and other inhomogeneities, J. Phys. A: Math. Gen. **31**, 2321 (1998).
[75] F. W. Strauch, Relativistic quantum walks, Phys. Rev. A **73**, 054302 (2006).
[76] S. E. Venegas-Andraca, Quantum walks: A comprehensive review, Quantum Inf. Process. **11**, 1015 (2012).
[77] T. D. Mackay, S. D. Bartlett, L. T. Stephenson, and B. C. Sanders, Quantum walks in higher dimensions, J. Phys. A: Math. Gen. **35**, 2745 (2002).
[78] B. Thaller, *The Dirac Equation*, Texts and Monographs in Physics (Springer-Verlag, Berlin, 1992).
[79] M. Reed and B. Simon, *Methods of Modern Mathematical Physics: Functional Analysis*, Methods of Modern Mathematical Physics No. 1 (Academic Press, San Diego, 1980).
[80] H. Sako, Convergence theorems on multi-dimensional homogeneous quantum walks, Quantum Inf. Process. **20**, 94 (2021).
[81] A. Ahlbrecht, H. Vogts, A. H. Werner, and R. F. Werner, Asymptotic evolution of quantum walks with random coin, J. Math. Phys. **52**, 042201 (2011).
[82] C. Di Franco, M. Mc Gettrick, and Th. Busch, Mimicking the probability distribution of a two-dimensional Grover walk with a single-qubit coin, Phys. Rev. Lett. **106**, 080502 (2011).
[83] N. Inui, Y. Konishi, and N. Konno, Localization of two-dimensional quantum walks, Phys. Rev. A **69**, 052323 (2004).
[84] H. Ohno, Parameterization of translation-invariant two-dimensional two-state quantum walks, Acta Math. Vietnam **43**, 737 (2018).
[85] C. Cedzich, A. Joye, A. H. Werner, and R. F. Werner, Exponential tail estimates for quantum lattice dynamics, Ann. Henri Poincaré (2024).
[86] Y. Baryshnikov, W. Brady, A. Bressler, and R. Pemantle, Two-dimensional quantum random walk, J. Stat. Phys. **142**, 78 (2011).
[87] Y. Higuchi, N. Konno, I. Sato, and E. Segawa, Spectral and asymptotic properties of Grover walks on crystal lattices, J. Funct. Anal. **267**, 4197 (2014).
[88] E. Segawa and A. Suzuki, Spectral mapping theorem of an abstract quantum walk, Quantum Inf. Process. **18**, 333 (2019).
[89] E. Segawa and A. Suzuki, Generator of an abstract quantum walk, Quantum Stud.: Math. Found. **3**, 11 (2016).
[90] K. Asahara, D. Funakawa, E. Segawa, A. Suzuki, and N. Teranishi, Spectral mapping theorem of an abstract non-unitary quantum walk, Lin. Alg. Appl. **676**, 1 (2023).
[91] T. Fuda, D. Funakawa, and A. Suzuki, Localization of a multi-dimensional quantum walk with one defect, Quantum Inf. Process. **16**, 203 (2017).